https://doi.org/10.5194/egusphere-2026-6638
Preprint. Discussion started: 10 November 2026
© Author(s) 2026. CC BY 4.0 License.

NO_x emissions changes from 2019 to 2021 in Eastern China as estimated through variational inversions and TROPOMI satellite data

Rimal Abeed[1,a], Audrey Fortems-Cheiney[2], Grégoire Broquet[1], Robin Plauchu[1], Isabelle Pison[1], Antoine Berchet[1], Elise Potier[2], Bo Zheng[3], Gaëlle Dufour[4], Adriana Coman[5], Dilek Savas[4], Guillaume Siour[5], Henk Eskes[6], Beatriz Revilla-Romero[7], Antony Delavois[8], and Philippe Ciais[1]

[1]Laboratoire des Sciences du Climat et de l'Environnement, CEA-CNRS-UVSQ, Gif-sur-Yvette, France
[2]Science Partners, Quai de Jemmapes, 75010 Paris, France
[3]Shenzhen Key Laboratory of Ecological Remediation and Carbon Sequestration, Institute of Environment and Ecology, Tsinghua Shenzhen International Graduate School, Tsinghua University, Shenzhen, 518055, China
[4]Université Paris Cité and Univ Paris Est Créteil, CNRS, LISA, F-75013 Paris, France
[5]Univ Paris Est Créteil and Université Paris Cité, CNRS, LISA, F-94010 Créteil, France
[6]Royal Netherlands Meteorological Institute (KNMI), De Bilt, the Netherlands
[7]GMV, Remote Sensing and Geospatial Analytics Division, Madrid, Spain
[8]European Space Agency (ESA), Rome, Italy

a: now at The Cyprus Institute, Climate and Atmosphere Research Center, 2121 Nicosia, Cyprus

Correspondence to: Rimal Abeed r.abeed@cyi.ac.cy

Abstract

China is one of the largest emitters of nitrogen oxides NO_x (= NO + NO_2) worldwide, and up-to-date estimates are crucial as the country faces rising pressure to curb emissions. We estimate NO_x emissions over Eastern China (101.75–132.25° E; 17.75–50.25° N) from 2019 to 2021, focusing on the impacts of COVID-19 and the Chinese Lunar New Year (LNY). Using high-resolution NO_2 observations from TROPOMI, onboard the Sentinel-5 Precursor satellite, our estimates are at the regional, national, and provincial scales. They are produced using the Community Inversion Framework (CIF), coupled to the CHIMERE regional chemistry transport model at 0.5° resolution. Our results show a drop in NO_x emissions of -35% during February 2020, as compared to 2019. The drop in NOx emissions is driven mostly by lockdown-related mobility restrictions and LNY festivities. Provincial reductions amounted to -15%, -16%, -17% in Hubei, Shanghai and Jiangsu respectively. Anthropogenic NOx emissions over Eastern China fell by 0.4 $TgNO_2$/year in 2020 vs. 2019, and by 0.2 TgNO2/year in 2021 compared to 2020. The yearly budget of NOx emissions for 2019, 2020 and 2021 are 18.3, 17.9, and 17.7 $TgNO_2$ respectively. Our estimates of recent past years offer insights to guide future strategies and policies to reduce NO_x emissions in China and its provinces. These results highlight the advantages of combining high dimensional variational inversion methods with high-resolution satellite data, to strengthen air quality monitoring and support more effective regulations.

1. Introduction

Besides being one of the most populated countries (1.4 Billion inhabitants in 2019 according to the Chinese census data (NBSC, 2023)), China's exports are the highest globally ($2.75T vs. $1.52T in the United States (U.S.) that comes next (OEC, 2022); China is the leading manufacturing country as it

https://doi.org/10.5194/egusphere-2026-6638
Preprint. Discussion started: 10 November 2026
© Author(s) 2026. CC BY 4.0 License.

accounted for 29% out of the global manufacturing output during 2023 (ChinaPower, 2025). Such industrial activities are directly linked to high levels of energy consumption and fossil fuel use (Abdelwahab et al., 2024). Since 2005, China has also been considered the main emitter of nitrogen oxides (NO_x= NO + NO_2) in the world, followed by the U.S. and then the European Union (Wang et al., 2022). Anthropogenic NO_x emissions are mainly driven by fossil fuel combustion, for instance due to transportation (Zheng et al., 2018) power plants (Tang et al., 2020), and some types of industrial processes (e.g. steel, iron and cement productions among others) (Bo et al., 2021; Liu et al., 2021). Agricultural activities, especially the application of nitrogen-based fertilizers, also yield large amounts of NOx emissions. In this study, we account for these NO_x agricultural soil emissions as a part of the anthropogenic emissions.

NO_x are air pollutants that are crucial to tropospheric chemistry. For instance, the photo-oxidation of NO_x is a major source of nitrous acid (HONO), the latter accelerates the formation of tropospheric ozone (O_3) (Song et al., 2023). O_3, when in the troposphere, is damaging to human health (Donzelli and Suarez-Varela, 2024) and to the ecosystem (Agathokleous et al., 2020). NO_x gases act as oxidizing agents and therefore intervene in the chemistry of volatile organic compounds (VOCs) (Atkinson, 2000). These gases have been linked to a variety of physical diseases (Soni et al., 2018). Due to their role in particulate matter (PM) formation and particle growth, NO_x gases were found to be linked to haze episodes in China (He et al., 2014). In addition to their impact on the environment, NO_x emissions are one of the drivers of the increase of premature death due to deteriorated air quality, with numbers of deaths that are expected to be higher in the future (Bressler, 2021). In a study carried out in the Netherlands, Zock et al. (2018) found a positive link between air pollution and diseases such as asthma, diabetes, headaches, among others; they included in their analysis pollution by PM ($PM_{2.5}$ <2.5 µm, and PM_{10} <10 µm) and NO_2 gas. The exposure to high amounts of NO_x gases increases the risk of mental health disorders (e.g., anxiety, depression, and even suicide attempts), as Shaw and Van Heyst (2022) showed a positive correlation between the risk ratio (referring to the increased risk linked to an increase of NO_2 concentration by 10 $\mu g \cdot m^{-3}$) and the exposure rate of NO_2. Ju et al. (2023) have also demonstrated the impact of NO_x-related air pollutants (O_3 and $PM_{2.5}$) on mental health in highly polluted cities over China.

In 2006, the Chinese government put in place the 11th 5-year plan (2006 – 2010) (NPC, 2006) to control air pollutants such as sulfur dioxide (SO_2) and PM. In 2011, NO_x control was added to the 12th 5-year plan (2011 – 2015), to reduce the annual Chinese NO_x emissions by 10% compared to 2010. And later in 2018, an action plan for a duration of three years was introduced. This plan aimed at reducing the emissions of both SO_2 and NO_x emissions gases by a minimum 15% as compared to 2015 (Li et al., 2023b). Chinese policies seem to succeed in reducing the NO_x emissions and therefore the NO_2 concentrations after 2010 (Ding et al., 2017a), and remarkably, the gross domestic product (GDP) started decoupling from the NO_x emissions in 2011 (Li et al., 2023b). Nevertheless, the decrease in NO_2 concentrations did not necessarily lead to an equivalent enhancement in air quality. Some studies argued that the alteration in the balance of the VOC/NO_x ratio did in fact lead to an increase in surface O_3 concentrations (Li et al., 2024b; Lu et al., 2023) causing haze episodes in Shanghai. An accurate account of NO_x emissions in space and time is needed to i) assess the effectiveness of policies aimed at reducing NO_x emissions and ii) to understand the impact of the evolution of NO_x emissions and of NO_2 concentrations on air quality.

https://doi.org/10.5194/egusphere-2026-6638
Preprint. Discussion started: 10 November 2026
© Author(s) 2026. CC BY 4.0 License.

The quantification of anthropogenic NO_x emissions following a bottom-up (BU) approach, based on the statistics of activity sectors and fuel consumption and relying on emission factors per activity type, suffers from relatively large uncertainties at the national and annual scales and bear, in addition to that, large spatial and temporal differences (Ding et al., 2017b; Jena et al., 2015). Saikawa et al. (2017) have compared five different inventories focusing on the estimates of Chinese NO_x emissions, including the Regional Emission inventory in ASia v2.1 (REAS), the Multi-resolution Emission Inventory for China (MEIC), the Emission Database for Global Atmospheric Research v4.2 (EDGAR), the inventory by Yu Zhao (ZHAO), and the Greenhouse Gas and Air Pollution Interactions and Synergies (GAINS). They have shown that large discrepancies between the BU estimates were mainly related to different statistical data and emission factors for the energy and transport sectors, as inventories used different provincial statistics (Saikawa et al., 2017). To develop accurate, high-resolution emission inventories, integrating independent information sources is essential. Atmospheric measurements can serve as a valuable complement to current BU approaches, thereby enhancing the spatial precision of emission inventories. These improvements are crucial for effectively assessing air quality policies.

Since the 2000s, NO_2 tropospheric concentrations have been monitored around the world by space-borne instruments, such as the Global Ozone Monitoring Experiment (GOME) (Burrows et al., 1999) and GOME-2 (Munro et al., 2016), the SCanning Imaging Absorption spectroMeter for Atmospheric CHartographY (SCIAMACHY) (Bovensmann et al., 1999; Burrows et al., 1999) and the Ozone Monitoring Instrument (OMI) (Levelt et al., 2018). In this context, attempts have been made to develop so-called top-down (TD) methods, complementary to BU inventories, to deduce NO_x emissions from NO_2 satellite data. The OMI NO_2 tropospheric vertical column densities (TVCDs) have been exploited previously to estimate NO_x emissions in China (Gu et al., 2014; Qin et al., 2023; Savas et al., 2023). For example, Savas et al. (2023) estimated the evolution of anthropogenic NO_x emissions in 2015 and 2019 compared to 2010 over Eastern China. They have found a decrease of NO_x emissions in the southern part of Eastern China over large urbanized and industrialized locations but an increase in the northern part in 2015 and 2019 compared to 2010.

The successor of OMI, the TROPOspheric Monitoring Instrument (TROPOMI) (Veefkind et al., 2012), on board the Copernicus Sentinel-5 Precursor (S-5P) satellite launched in 2017, has brought images of NO_2 with higher spatial resolution (pixel size of about 3.5 km × 5.5 km since August 2019). With a swath as wide as approximately 2600 km on ground, TROPOMI also provides daily coverage. This higher spatial resolution increases the potential to quantify local emissions (from specific provinces, urban or industrial areas, sometimes from specific large industrial sites). It also supports improved precision in NO_x emission estimates at large scales by offering better insights into spatial heterogeneity in chemistry and emission processes (e.g., industrial vs. urban areas) at fine scales.

Both OMI and TROPOMI NO_2 observations have also been used to quantify the impact on NO_2 concentrations of the Lunar New Year national holiday (LNY), which is a 7 to 14-days of celebration with businesses and factories closed that takes place every year around late January – mid February (Bauwens et al., 2020; Chu et al., 2021; Cooper et al., 2022; Pei et al., 2020; Tan et al., 2009). By the end of 2019, and in the middle of the 3-year action plan (2018 – 2020), the COVID-19 pandemic broke in Wuhan. The latter is one of the multiple megacities in China that hosted 11.21 million inhabitants in 2019 (HKTDC, 2026). As a response to the increasing rates of infections and deaths caused by the COVID-19 virus, the Chinese government implemented strict mobility regulations across various

https://doi.org/10.5194/egusphere-2026-6638
Preprint. Discussion started: 10 November 2026
© Author(s) 2026. CC BY 4.0 License.

provinces starting early 2020 and extending until early April 2020 in some cases. The applied measures varied based on the number of infection cases reported (Chinazzi et al., 2020; Li et al., 2020). For instance, in Wuhan, a full 76-day lockdown was imposed, the longest in China, and it extended from the 23rd of January 2020 up until the 8th of April 2020. In other Chinese cities, shorter lockdown periods accompanied by lighter measures were imposed, the periods varied between 3 and 60 days. Due to the reduction in mobility and the stay-home rule imposed by the Chinese government, the NO_2 TVCDs and the NO_x emissions were expected to have significantly dropped during the period of the lockdown (Bauwens et al., 2020; Ding et al., 2020; Levelt et al., 2022; Li et al., 2024a, 2023c; Zhang et al., 2019).

If all the inverse modeling studies about the COVID-19 crisis agree that NO_x emissions were indeed reduced during the lockdown period in 2020 (Ding et al., 2020; He et al., 2022; Li et al., 2024a; Wei et al., 2023; Zhang et al., 2019, 2020), they differ on the extent of these reductions. The simplest approaches extrapolate the relationship between the tropospheric concentrations and the emissions from a single perturbation of the emissions in the CTM simulations, and from the assumption that this relationship is purely local (occurring within the scale of the CTM grid cell)(Li et al., 2024a; Zheng et al., 2021). These simplifications and assumptions provide a limited capability to account for the chemistry. A more detailed account of the complex NO_x chemistry with more elaborate approaches using chemistry-transport models (CTMs) with ensemble Kalman filter inverse modelling techniques or variational approaches should support more accurate derivations of NO_x emissions from NO_2 satellite data.

In this study, we leverage the high spatial resolution and extensive coverage of NO_2 tropospheric columns provided by TROPOMI instrument, onboard the Sentinel 5-Precursor satellite, to estimate NO_x emissions in Eastern China, where the Chinese NO_x emissions are the highest, at the relatively high horizontal resolution of 0.5°×0.5° for the period 2019 – 2021, that includes changes in emissions due to Chinese emissions reduction policies, lockdown measures, and LNY holidays. The relatively fine spatial resolution makes it possible to estimate the decrease/increase of NO_x emissions down to the provincial level. We therefore study the impact of COVID-19 lockdown measures, as well as the effect of the LNY on the emissions of NO_x in a total of 26 provinces over Eastern China. To estimate these emissions, we conduct variational inversions at 0.5° and 1-day resolution with the Community Inversion Framework (CIF, (Berchet et al., 2021)), using the CHIMERE CTM (Menut et al., 2024), including a chemistry module taking into account the complex NO_x chemistry in gas-phase, its non-linearities, and its adjoint (Fortems-Cheiney et al., 2021). This framework and the regional inversion configuration are built upon the work done by Fortems-Cheiney et al. (2021, 2025), Savas et al. (2023) and Plauchu et al. (Plauchu et al., 2024). **Section 2** presents the data sources and pre-processing, as well as the regional inverse modelling configuration. **Section 3** presents the results and discusses them, and the last section summarizes the conclusions.

2. Data and Methods

2.1. Configuration of the CHIMERE CTM for the simulation of NO_2 concentrations in Eastern China

https://doi.org/10.5194/egusphere-2026-6638
Preprint. Discussion started: 10 November 2026
© Author(s) 2026. CC BY 4.0 License.

Study domain boundaries	101.75-132.25°E; 17.75-50.25°N
Horizontal resolution	0.5°×0.5°, 61 × 65 grid cells (longitude × latitude), i.e., 3965 grid cells per level
Vertical resolution	17 layers extending from the surface up to 200 hPa (around 12 km above the sea level)
Meteorological fields	European Centre for Medium-Range Weather Forecasts (ECMWF) operational meteorological forecast (Owens and Hewson, 2018)
Initial and boundary conditions (excluding NO_x)	LMDZ-INCA (Szopa et al., 2009)
Anthropogenic emissions	CAMS-GLOB-ANT-v5.3
Natural soil emissions (NO+VOCs)	CAMS-GLOB-SOIL for NO (Simpson et al., 2021) and Model of Emissions of Gases and Aerosols from Nature (MEGAN) for VOCs (Guenther et al., 2006)
Chemical Scheme	MELCHIOR-2 (Carter, 1990; Derognat et al., 2003)

Table 1. The configuration of CHIMERE for the simulation of NO_2 concentrations in Eastern China. See **Figure 1** for a map of the domain. MELCHIOR-2: Modèle Lagrangien de Chimie de l'Ozone à l'échelle Régionale, gas-phase chemical reaction scheme.

CHIMERE CTM is designed for the study of regional atmospheric pollution events (Ciarelli et al., 2019; Menut et al., 2020) and is part of the operational ensemble of the Copernicus Atmosphere Monitoring Service (CAMS) regional services. The long series of publications on air quality modelling with this CTM, including comparisons to observations, support the reliability and the accuracy of the CHIMERE simulations over regions such as Eastern China. In particular, C. Gao et al. (2024) showed that CHIMERE provides reliable simulations of air quality and NO_2 concentrations over this region, effectively capturing annual and seasonal spatiotemporal characteristics when evaluated against surface and satellite observations.

The configuration set for the CHIMERE simulations in this study is summarized in **Table 1**. CHIMERE is driven here by meteorological fields at a fine resolution of 0.25°, from the European Centre for Medium-Range Weather Forecasts (ECMWF) operational meteorological forecast (Owens and Hewson, 2018). The MELCHIOR-2 scheme includes 120 oxidation reactions of 40 gaseous species.

https://doi.org/10.5194/egusphere-2026-6638
Preprint. Discussion started: 10 November 2026
© Author(s) 2026. CC BY 4.0 License.

183



Figure 1. The study domain covers the Chinese provinces of mainland China, hereafter called "Eastern China". The model grid cells are shown in dashed grey.

184 Considering the short lifetime of NO_2, we do not consider its influx from outside the domain: its
185 boundary conditions are set to zero, as in Savas et al. (2023), Plauchu et al. (2024) and in Fortems-
186 Cheiney et al. (2024) . Nevertheless, the lateral and top boundaries for other species, such as O_3, nitric
187 acid (HNO_3), peroxyacetyl nitrate (PAN) and formaldehyde (HCHO), participating in the NO_x
188 chemistry are considered, as in Savas et al. (2023), in Plauchu et al. (2024) and in Fortems-Cheiney et
189 al. (2024). In this study, Eastern China refers to the Chinese mainland included in the study domain
190 (**Figure 1**).

191 **2.2. Prior estimates of NO_x emissions in Eastern China**

192 The main goal of an inversion is to correct a-priori emission maps, that we refer to as "prior"
193 emissions/estimates. The NO_x anthropogenic prior estimates in this study come from the CAMS-
194 GLOB-ANT-v5.3 gridded inventory (Soulie et al., 2024), mapping global NO_x emissions at a 0.1°x0.1°
195 horizontal resolution. The impact of the 2020 lockdown is considered in this inventory. NO_x emissions

https://doi.org/10.5194/egusphere-2026-6638
Preprint. Discussion started: 10 November 2026
© Author(s) 2026. CC BY 4.0 License.

are expressed in either teragram or kiloton in equivalent NO_2 ($TgNO_2$ or $ktNO_2$) throughout the study. NO_x soil emissions from agriculture are included in CAMS-GLOB-ANT-v5.3.

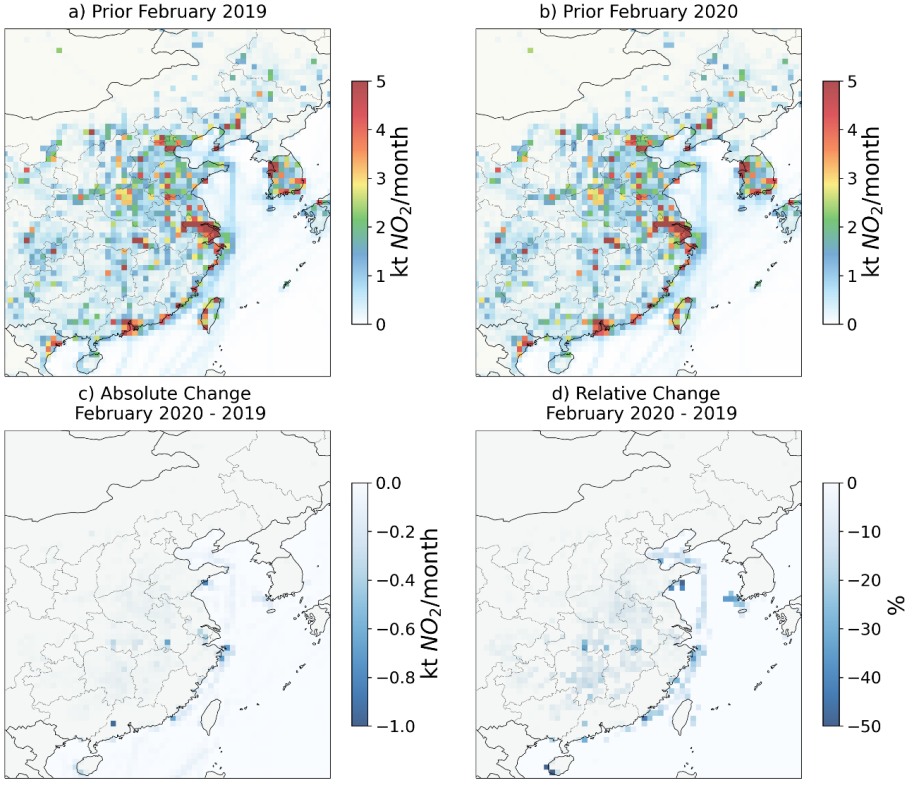


Figure 2. Prior estimates of anthropogenic NO_x emissions for February 2019 (a) and 2020 (b), and the absolute (c) and relative (d) change between these estimates. The total relative difference across the entire domain (shown in panel d) is –22%.

In addition to NO_x anthropogenic emissions, NO natural emissions from soil are considered. Visser et al. (2019) have shown a strong underestimation of the NO_x natural emissions from MEGAN in summer over Europe, therefore, for this version of the product we use CAMS-GLOB-SOIL. Consequently, the NO_x prior natural emissions are here derived from the CAMS-GLOB-SOIL product (Simpson et al., 2021). Soil NO emissions in CAMS-GLOB-SOIL are represented as the sum of four different sources: FSoil = FBiome + FFert + FNdep + FPulse. Where FBiome is the background natural soil NOx flux driven by microbial nitrification and denitrification processes. FFert represents the additional NOx flux resulting from the application of nitrogen-based fertilizers (excluded in our analysis). FNdep accounts for the indirect contribution of atmospheric nitrogen deposition (wet and dry deposition). Finally, FPulse captures the transient, short-lived enhancement in NO emissions that occur when previously desiccated soils are rewetted. Soil emissions from agricultural activities are included in the CAMS-GLOB-ANT inventory, therefore, we do not use the FFert estimates from CAMS-GLOB-SOIL, to avoid a double-counting of the emissions due to fertilization. The lightning-generated NOx are not considered in the prior estimation. In China, the lightning-produced NO_x (LNO_x) emissions are estimated at 516 to 1054

https://doi.org/10.5194/egusphere-2026-6638
Preprint. Discussion started: 10 November 2026
© Author(s) 2026. CC BY 4.0 License.

ktNO2.yr^{-1} (Li et al., 2023a), and they contribute up to 7.5% to the total tropospheric NOx emissions (Fengxia et al., 2016). Fire emissions are also neglected, as their contribution to the NOx total emissions in China is relatively small 230 (50–450) ktNO2.yr^{-1} (Yin et al., 2019), which amounts to approximately 1.15% of the total national NO_x emissions. All the emission data are spatially aggregated at the horizontal resolution of 0.5°×0.5° of the CHIMERE grid.

2.3. NO_2 TVCDs from TROPOMI

In this study we use NO_2 TVCDs from the TROPOMI instrument (Veefkind et al., 2012). TROPOMI is a nadir-viewing hyperspectral spectrometer that covers a large spectral range (270 – 2385 nm) from the ultraviolet (UV) to the shortwave infrared (SWIR) (Lambert et al., 2025). S-5P follows a sun-synchronous polar orbit and has a daily overpass at 13:30 solar local time. TROPOMI has a swath of ~2600 km, with a spatial resolution of 3.5×5.5 km² (since 6 August 2019, and 3.5×7 km² prior to that time), and it provides near-global coverage.

We use reprocessed (RPRO) version 02.04.00 from TROPOMI NO_2 products, from January 2019 to December 2021. The main update in this version, compared to previous versions, is that it uses a spectral surface reflectivity climatology derived from TROPOMI (Tilstra et al., 2024) replacing the older OMI and GOME-2 (the Global Ozone Monitoring Experiment-2) datasets used in versions 1.0.2 to 2.3.1. This replacement, which also accounts for the directionality of the Lambertian Equivalent Reflectivity (LER), leads to significant changes in the cloud retrievals (Van Geffen et al., 2022).

TROPOMI RPRO-v02.04.00 data and ground-based MAX-DOAS data, from 31 stations globally, continue to show discrepancies that vary with the level of pollution near the station (Lambert et al., 2025). However, when MAX-DOAS profile data are vertically smoothed using the S-5P averaging kernels (AKs), the bias is positive (+10%) over non-polluted areas and negative (-32%) over highly polluted areas. Furthermore, comparisons of NO_2 total columns with the Pandora direct-sun spectrometer (Herman et al., 2009), which provides robust column measurements due to its trivial light path, show a median bias of -8% overall, with a positive bias of 4% at clean, high-altitude sites and a negative bias of -15% in polluted areas (Lambert et al., 2025). These biases are reduced when AKs are used, as in this study. We select data with a quality assurance (qa value) above 0.75, following the criteria of Lambert et al. (Lambert et al., 2025).

https://doi.org/10.5194/egusphere-2026-6638
Preprint. Discussion started: 10 November 2026
© Author(s) 2026. CC BY 4.0 License.

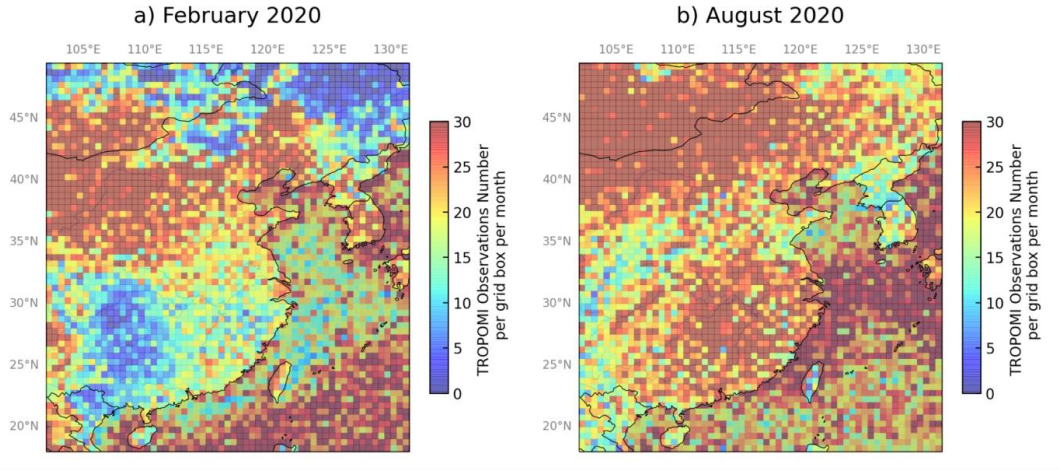


Figure 3. Number of TROPOMI super-observations (with a quality flag qa > 0.75) of tropospheric NO_2 (cloud-free) per 0.5° resolution grid-cell, during a winter month (a) and a summer month(b) in 2020.

In winter, some areas have a relatively lower observation number, as compared to the rest of the domain and to summer months (**Figure 3**). This is mainly due to the larger cloud cover, but other factors have an impact, such as the solar zenith angle, aerosol optical thickness and surface albedo (Gao et al., 2023) . In the case of a limited number of satellite observations per grid cell and per month, the inversion system will rely on, or stay close to, the prior estimates provided; there will be a lack of reduction of the uncertainties from the prior estimate in those grid cells and during the corresponding month (Li et al., 2025; Qin et al., 2023). TROPOMI provides reliable and consistent coverage of the studied domain, during summer months more than winter months, which makes it possible to estimate emissions down to the provincial level, while being aware of the possible uncertainties over certain grids most notably during winter.

2.4. Consistent comparison between simulated and observed NO_2 TVCDs

In order to compare NO_2 TVCDs simulated by CHIMERE with those provided by TROPOMI observations, we need to tackle several differences between the satellite instrument and the CTM 3D simulated NO_2 concentration fields. For example, these differences include: 1) spatial and temporal resolutions, and 2) variations of the instrument retrieval sensitivity to the concentrations along the vertical columns characterized by the retrieval AKs. A “super-observation” approach (Eskes et al., 2003; Miyazaki et al., 2012) is employed to aggregate the observations and derive errors (uncertainties from the retrieval process, including the propagation of the instrumental noise) and vertical sensitivity at the model resolution (Fortems-Cheiney et al., 2021; Plauchu et al., 2024; Savas et al., 2023). The temporal resolution is addressed, by matching the overpass of the S-5P satellite to the time stamps in the simulated TVCDs from CHIMERE. At a given time, in each model grid-cell covered by TROPOMI observations, the super-observation is defined as the observation (TVCD, errors and AKs) corresponding to the TVCD value closest to the mean of all the observations within this 0.5°×0.5° grid cell, and within the corresponding CHIMERE physical time step of approximately 5 to 10 minutes,

https://doi.org/10.5194/egusphere-2026-6638
Preprint. Discussion started: 10 November 2026
© Author(s) 2026. CC BY 4.0 License.

following the method described by (Plauchu et al., 2024). The simulated NO_2 TVCDs (**Figure 4**a, d for two months) broadly capture the spatial and temporal variabilities of those provided by TROPOMI (**Figure 4**c, f).

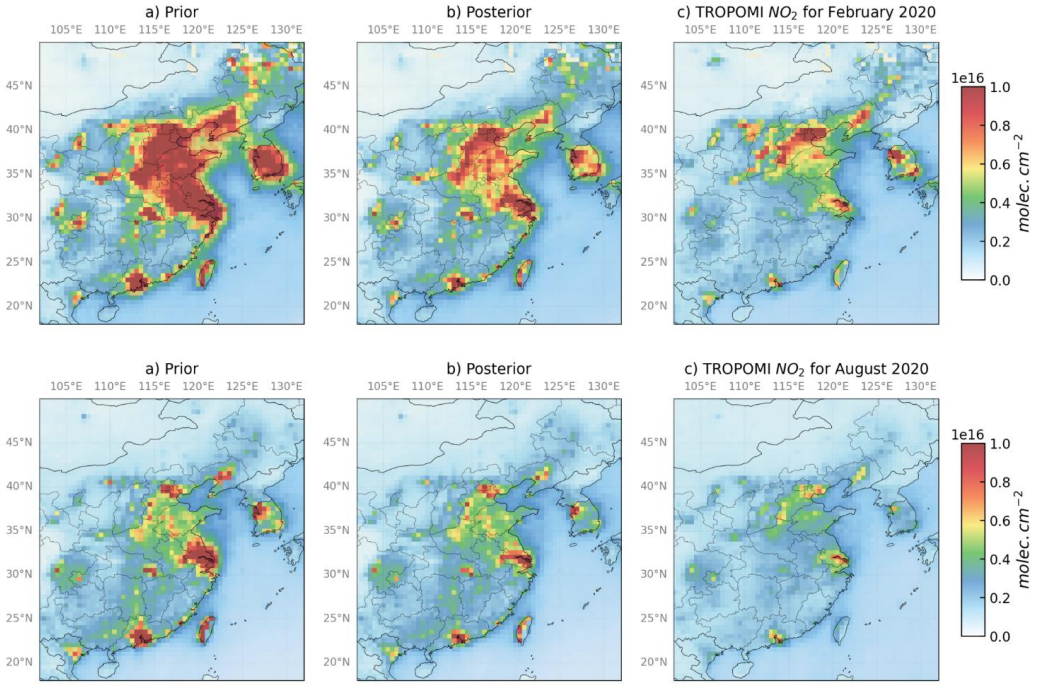


Figure 4. Monthly means of the NO_2 TVCDs correspond to the TROPOMI super-observations at 0.5° resolution during February (upper row) and August (bottom row) 2020. The CHIMERE prior TVCDs are shown in the first column (a, d), the posterior estimates using the correction of the prior are shown in the second column (b, e), and the TVCDs from TROPOMI are shown in the last column (c, f).

2.5. Variational inversion of NO_x anthropogenic and natural soil emissions

The NO_x emission estimates from the inversion (called "posterior" estimate of the emissions) consist in a correction of the prior estimates of NO_x emissions (described in **Section 2.2**), which reduce the differences between the simulated NO_2 and the TROPOMI NO_2 super-observations. We use a Bayesian variational inversion framework, similar to the one used in Fortems-Cheiney et al. (2021, 2024), Savas et al. (2023) and Plauchu et al. (2024). To cover the period from 2019 to 2021, we conduct a series of monthly inversions (covering 1-month windows) that are later combined; each inversion is independent of the others. In each iteration, the posterior emissions are derived from the minimization of the cost function $J(x)$, stated below as **Equation 1**:

https://doi.org/10.5194/egusphere-2026-6638
Preprint. Discussion started: 10 November 2026
© Author(s) 2026. CC BY 4.0 License.

$$J(x) = ½ \left(x - x^b\right)^T B^{-1}\left(x - x^b\right) + ½ \left(H(x) - y\right)^T R^{-1}\left(H(x) - y\right) \qquad \textit{Equation 1}$$

290

291 The control vector $\boldsymbol{x}$, contains variables that are corrected by the inversion, which, here, all underlay
292 the estimates of the surface emissions of NO and NO_2 in input of CHIMERE, while $\boldsymbol{x^b}$ is the prior
293 estimates of the control vector. $\boldsymbol{y}$ combines the TROPOMI super-observations. $\boldsymbol{H}$, the observation
294 operator, links the variables in the control vector (log-space) to the observation space defined by the
295 TROPOMI super-observations. It includes: the exponential operator and scaling of the prior emission
296 maps that convert the maps of the logarithm of the coefficient for the emission into emission maps at
297 the spatial and temporal resolutions of CHIMERE; the atmospheric chemistry and transport model
298 CHIMERE itself; and the extraction of the TVCDs from CHIMERE when TROPOMI super-
299 observations are available (spatially and temporally).

300 $\boldsymbol{B}$ is the prior error covariance matrix: it fully characterizes the uncertainty in $\boldsymbol{x^b}$, called prior uncertainty
301 under the assumption that it follows an unbiased and normal distribution N(O,**B**); $\boldsymbol{R}$ is the observation
302 error covariance matrix: it corresponds to the sum of uncertainties from the observation operator and
303 from the super-observations; assuming that these errors have an unbiased and normal distribution,
304 N(0,$\boldsymbol{R}$), they are fully characterized by $\boldsymbol{R}$.

305 Here, $\boldsymbol{x}$ is built so that the uncertainties in the prior estimates of the emissions are implicitly modelled
306 assuming that they have a log-normal distribution, in order to reflect the uncertainty in the order of
307 magnitude of these emissions and forcing the analyzed emissions to be positive (Plauchu et al., 2024).
308 $\boldsymbol{x}$ is thus composed of logarithms of scaling coefficients to be applied to the prior estimate of the
309 emissions.

310 $\boldsymbol{x}$ is split according to the anthropogenic and natural components of the NO and NO_2 emissions in each
311 of the model grid cells at 0.5° resolution for each day. The information provided by the TROPOMI
312 observations, together with the spatial and temporal resolutions of CHIMERE, do not support an
313 accurate separation of the total NO_x emissions between NO and NO_2 emissions. However, the control
314 vector $\boldsymbol{x}$ maintains this separation for technical simplicity, as this approach does not adversely impact
315 the estimation of the total NO_x emissions. There is no further sectorization of the control of
316 anthropogenic emissions. More specifically, $\boldsymbol{x}$ consists of:

317 - the logarithms of the scaling coefficients for NO anthropogenic emissions, at a 1-day temporal
318 resolution, and a 0.5°×0.5° (longitude, latitude) horizontal resolution; and over the 17 vertical
319 layers of CHIMERE
320 - the logarithms of the scaling coefficients for NO_2 anthropogenic emissions, at the same vertical,
321 temporal, horizontal resolutions as for NO,
322 - the logarithms of the scaling coefficients for NO natural soil emissions at a 1-day temporal
323 resolution, and a 0.5°×0.5° (longitude, latitude) horizontal resolution at the surface (1 vertical
324 layer).

325 Accordingly, $\boldsymbol{B}$, is block-diagonal matrix with three blocks: the first block corresponds to the
326 logarithms of the NO anthropogenic emissions, in which each diagonal element is set at $(0.35)^2$, this
327 variance value in the log-space corresponds to a factor ranging between 70 to 140% in the emission

https://doi.org/10.5194/egusphere-2026-6638
Preprint. Discussion started: 10 November 2026
© Author(s) 2026. CC BY 4.0 License.

space, at the 1-day and model's grid scale. Similarly, the second block corresponds to the logarithms of the NO_2 anthropogenic emissions, in which each diagonal element is set at $(0.35)^2$, this variance value in the log-space corresponds to a factor ranging between 70 to 140% in the emission space, at the 1-day and model's grid scale.

The third block of $\boldsymbol{B}$ is set for NO natural soil emissions, in which each diagonal element is set at $(0.5)^2$, corresponding to a factor ranging between 60 to 164% in the emission space at the 1-day and model's grid scale.

We account for spatial correlations in the uncertainties both for anthropogenic and natural parts. Spatial correlations are described by exponentially decaying functions with an e-folding length of 50 km over land and over the sea as in Fortems-Cheiney et al. (2025). However, we do not account for temporal correlations between different days.

The uncertainties on the observations y and on the observation operator $\boldsymbol{H}$ are characterized by the so-called observation error covariance matrix $\boldsymbol{R}$, set up here as a diagonal matrix based on the assumption that these errors are not correlated in space or time when aggregated at the model 0.5° and 1 h resolution. The variance in the observation errors corresponding to individual observations in the diagonal of $\boldsymbol{R}$ is the quadratic sum of the error we have assigned to the TROPOMI super-observations and of an estimate of the errors from the observation operator. We assume that the observation operator error is dominated by the chemistry-transport modelling errors and -in case when the model grid-cell is covered by few TROPOMI observations- by the errors associated with the discrepancies between the spatial representativeness of the super-observations and of the model corresponding column. The error associated with each super-observation therefore corresponds to the maximum between two values: 20% of the simulated NO_2, and 20% of the bias between the observed NO_2 and the simulated NO_2 ($TROPOMI\ superobservation\ NO_2 - CHIMERE\ simulated\ NO_2$).

The inversion system searches for the minimum of the cost function $\boldsymbol{J}$ using the iterative M1QN3 limited-memory quasi-Newton minimization algorithm (Gilbert & Lemaréchal, 1989). At each iteration, the computation of the gradient of $\boldsymbol{J}$ relies on the adjoint of CHIMERE, which is the adjoint of the observation operator. We impose a reduction of the norm of the gradient of $\boldsymbol{J}$ by 90% as a constraint for the interruption of the minimization process.

3. Results

3.1. Improving the fit between CHIMERE simulations and TROPOMI super-observations

Before analyzing the results in terms of NO_x emissions, we check the behavior of the inversion by comparing the performance of the prior and posterior simulations in reproducing the spatial and temporal variations of the observations. We analyzed the months of February and August 2020 to illustrate the typical behavior of the inversions in winter and summer months, but the analysis is performed on all the months for the years 2019, 2020 and 2021 (not shown here).

TROPOMI super-observations and the corresponding CHIMERE NO_2 TVCDs present similar spatial patterns, with hotspots over Henan, Beijing, Wuhan, and Hong Kong, as well as in the Northeastern

https://doi.org/10.5194/egusphere-2026-6638
Preprint. Discussion started: 10 November 2026
© Author(s) 2026. CC BY 4.0 License.

province, Liaoning (**Figure 4**). However, the prior simulation overestimates the NO_2 TVCDs in Eastern China compared to the observations, with a mean bias of about +30% and +12% for February and August 2020 respectively.

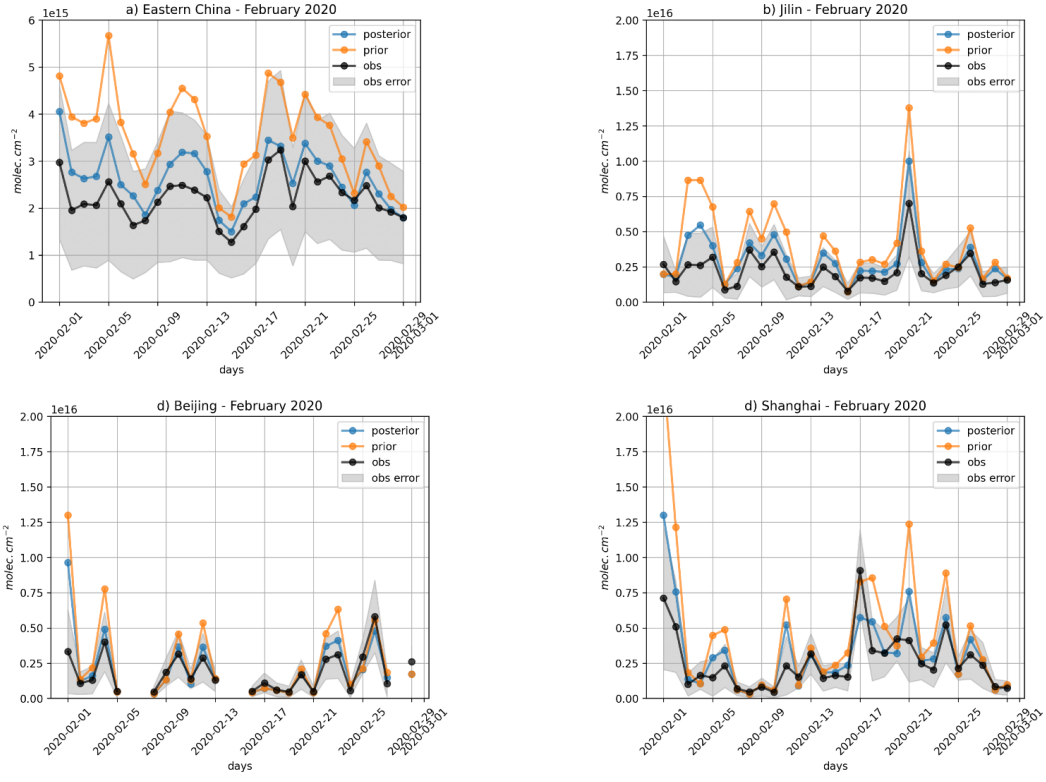


Figure 5. Daily mean posterior (blue) and prior (orange) estimations of NO_2 TVCDs as compared to that of the TROPOMI super-observations (obs, black) during February 2020, with the 1-sigma error associated to the super-observations as a grey shaded area (obs error). The top row features averages for Eastern China (a) and the province of Jilin (b), and the bottom row shows averages for the provinces of Beijing (c) and Shanghai (d). The NO_2 TVCDs are expressed in molecules.cm^{-2}. Note that the y axis limits are different for the provinces as compared to Eastern China. The provinces are shown in Figure 1 on the map of the domain.

The inversion brings the simulated NO_2 TVCDs closer to the TROPOMI super-observations (**Figure 4**; see also the time series of daily mean TVCDs in **Figure 5**). The improvement of the fit between the simulated and the observed NO_2 differs among polluted and rural regions, for instance, it is the best over polluted regions such as Henan, Beijing, Wuhan, Hong Kong, and Liaoning (**Figure 4**). Nevertheless, the posterior simulation still presents positive biases compared to the observations (**Figure 4** and **Figure 5**). This is partly due to 1) the limitations in the spatial and temporal coverage of TROPOMI, particularly in winter (**Figure 3**), 2) the errors associated with TROPOMI super-observations and with the CTM (assigned in the ***R*** matrix, **Section 2.5**), and 3) the potential lack of sensitivity of NO_2 TVCDs to NO_x emissions depending on the chemical regime. As the CHIMERE prior simulation overestimates the NO_2 TVCDs, the inversion brings the CHIMERE NO_2 columns closer to the TROPOMI data by reducing NO_x emissions (**Figure 6, Section 3.2**).

https://doi.org/10.5194/egusphere-2026-6638
Preprint. Discussion started: 10 November 2026
© Author(s) 2026. CC BY 4.0 License.

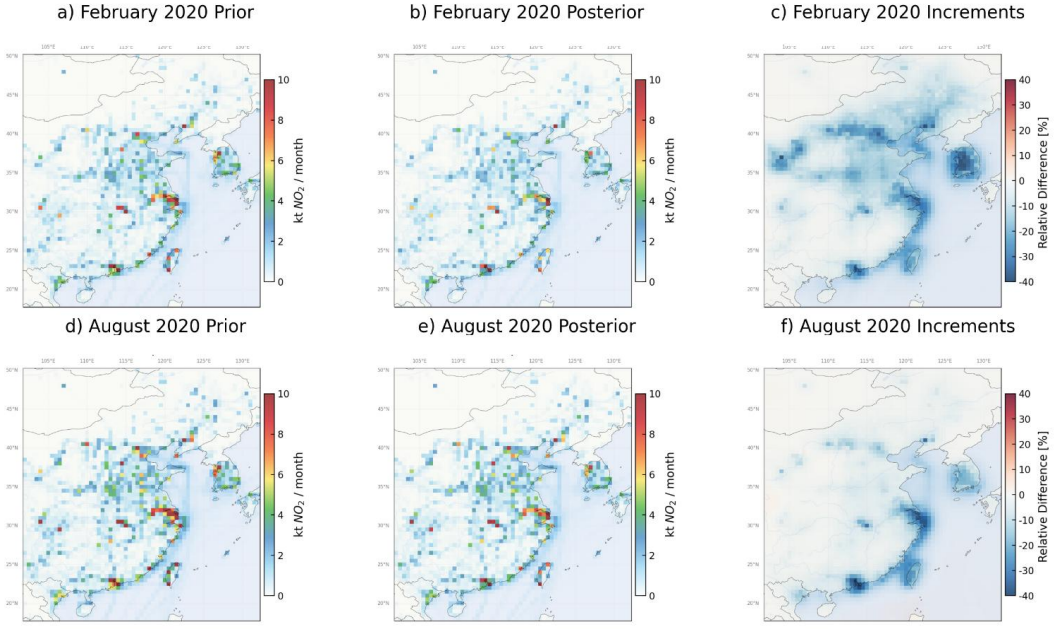


Figure 6. NO_x emissions during the months of February (top, a to c) and August (bottom, d to f) 2020. The prior (a, d) and the posterior (b, e) estimates are expressed in kilotons equivalent NO_2 ($ktNO_2$/month), and the relative increments (c, f) to the prior emissions from the inversion, in %.

3.2. Anthropogenic NO_x annual budgets in Eastern China from 2019 to 2021

This section focuses on comparing the anthropogenic posterior NO_x emission estimates and the prior ones. NO_x posterior total emissions over Eastern China were reduced by − 10.3% to 11.4% compared to the prior inventory, for all years considered here (**Figure 7**). This result may be partly due to the artificial propagation of errors from the TROPOMI observations ((Lambert et al., 2025); **Section 2.3**) and from the CTM. Nevertheless, the potential biases of the TROPOMI observations are considered in the characterization of our **R** matrix (**Section 2.5**). In addition, CHIMERE has been shown to be reliable for simulating air quality over Eastern China (Gao et al., 2024) and no large-scale modeling bias has been identified in the CHIMERE simulation of NO_2 concentrations. Our results therefore suggest that NO_x emissions are overestimated by the prior inventory.

The inversions show a small decrease of NOx emissions of about -2.2% between 2019 and 2020, consistent in sign with the prior estimates (-1%, Table 2). Over the 3-year period, emissions decrease by -3.2%, which includes a decrease of NOx emissions in 2020 due to COVID-19 lockdown (Section 3.4) and an additional decrease of -1% in 2021, compared to 2020. This decrease in 2021 is consistent with Li et al. (2025) and ABaCAS-EI v2.0 (Li et al., 2023b).

https://doi.org/10.5194/egusphere-2026-6638
Preprint. Discussion started: 10 November 2026
© Author(s) 2026. CC BY 4.0 License.

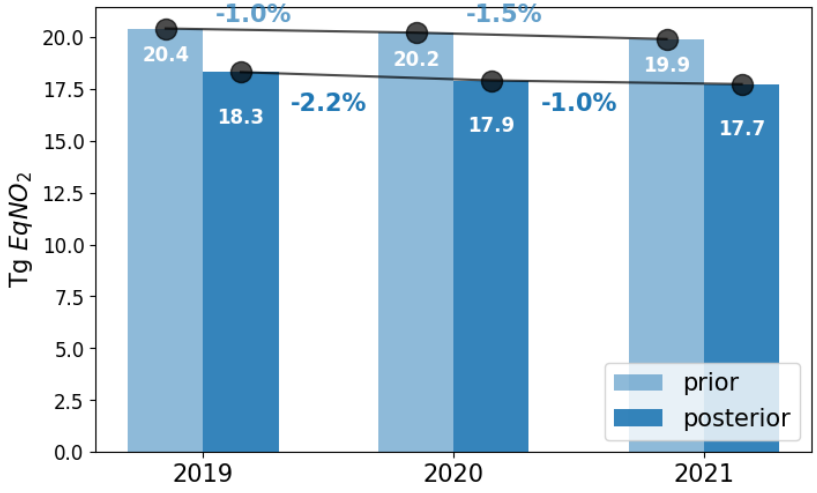


Figure 7. Annual anthropogenic NO_x emissions for the period 2019 – 2021, expressed in Tg $EqNO_2$/year for Eastern China in the domain of study. The prior (light blue) and posterior (dark blue) total estimates are shown in white on each bar. The year-on-year changes are shown in percentage above the black lines.

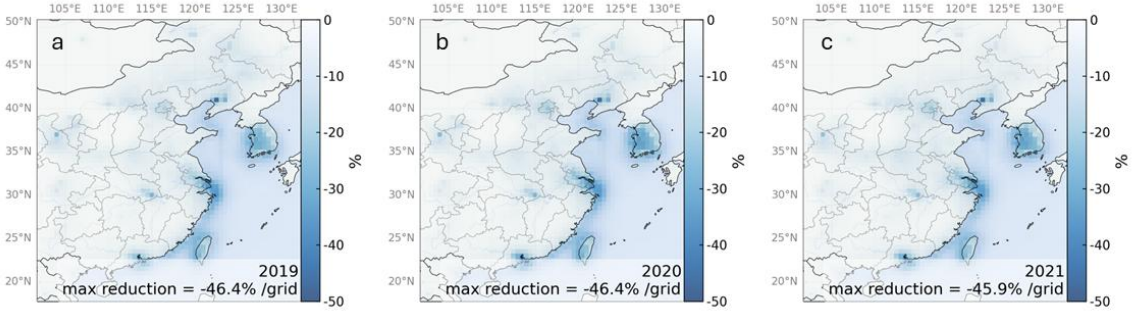


Figure 8. Maps of the yearly increments relative to the prior estimates (%) of annual NO_x emissions at a 0.5° resolution, for the years 2019 to 2021 (a to c).

At the scale of the province, the largest negative increments over the 3-year period are obtained in four main provinces: Liaoning (-25%), Shanghai (-27%), Jiangsu (-18%), and Guangdong (-17%). At the grid-cell resolution, however, the reduction of the prior estimates is highly correlated (r>0.97) to the prior estimates. Similar results are found in the study of Plauchu et al. (Plauchu et al., 2024) over France, with strong corrections mainly over dense urban areas. The corrections applied to the prior estimates in Eastern China, on a yearly scale are similar inter-annually, and they reach up to -46% in 2019, 2020, and 2021, per grid box and per year (Figure 8). The robustness of the computation of uncertainties in the posterior emission estimates highly relies on the accuracy in the characterization of the uncertainties in the observations (TROPOMI TVCDs), in the CTM (CHIMERE), and in the prior emission estimates (CAMS-GLOB-ANT-v5.3). Therefore, major challenges resurface when characterizing the types of covariance associated with these uncertainties and, for certain components, when quantifying their local amplitudes and temporal variations. This issue was discussed in other studies, especially regarding NO_2 observation datasets and validation (Liu et al., 2024; Rijsdijk et al., 2025). Due to all the reasons mentioned, comparing inverse modelling results with other inventories or

https://doi.org/10.5194/egusphere-2026-6638
Preprint. Discussion started: 10 November 2026
© Author(s) 2026. CC BY 4.0 License.



independent studies is currently the most reliable approach to assess the robustness of our method. We compared our anthropogenic NO_x estimates with other inventories at the yearly and monthly scales, and we present some of these comparisons in **Table 2** (yearly) and **Table 3** (monthly). At the yearly scale, our posterior emissions are the closest to those provided by DECSO (van der A and Ding, 2025), followed by ABaCAS-EI v2.0 inventory (Li et al., 2023b). ABaCAS-EI v2.0 inventory does not provide monthly emissions estimates, only yearly, per sector and per province from 2005 to 2021. When compared to DECSO (van der A and Ding, 2025), we found that our posterior estimates for 2019, 2020 and 2021 are lower by −7.5%, −3.3% and −6.5% respectively (**Table 2**). Regarding the annual variability, DECSO and our posterior estimates both capture the LNY dip in NO_x emissions, as well as the peak in December 2019. DECSO shows a peak during summer months that we do not observe in our posterior estimates, and it is 13% to 22% higher than our posterior estimates from November to January (**Table 3**).

China	2019	2020	2021	Reference
prior	**20.4**	**20.2**	**19.89**	This study
posterior	**18.3**	**17.9**	**17.72**	This study
ABaCAS-EI v2.0	16.94 (+8.0%)	16.24 (+10.2%)	15.79 (+12.2%)	(Li et al., 2023b)
DECSO	19.78 (-7.5%)	18.51 (-3.3%)	18.96 (-6.5%)	(van der A and Ding, 2025)

Table 2. Comparison of yearly NO_x estimates with other studies. The data shown is for China and is in Tg NO_2/year. The percentages shown in parentheses are the relative differences of our posterior estimates with respect to each dataset, (posterior – dataset) ×100 / dataset.

Month	prior	posterior	DECSO	%
January	1.78	1.52	1.95	-22.10%
February	1.38	1.21	1.22	-1.08%
March	1.67	1.55	1.60	-3.30%
April	1.55	1.49	1.63	-8.31%
May	1.63	1.57	1.68	-6.61%
June	1.65	1.57	1.74	-10.01%
July	1.79	1.63	1.67	-2.67%
August	1.79	1.58	1.43	+10.20%
September	1.71	1.52	1.43	+6.36%
October	1.70	1.54	1.64	-6.27%
November	1.81	1.54	1.78	-13.39%
December	1.98	1.62	1.99	-18.69%
Yearly budget	20.44	18.34	**19.76**	-7.2%

Table 3. Comparison of monthly NO_x estimates with other studies, for 2019. The data shown is for China and is in Tg NO_2/month. The percentages shown next to DECSO-v6.5-TROPOMI are the relative difference with our posterior estimates.

https://doi.org/10.5194/egusphere-2026-6638
Preprint. Discussion started: 10 November 2026
© Author(s) 2026. CC BY 4.0 License.

3.3. Seasonal cycle of NO_x and the Lunar New Year contribution

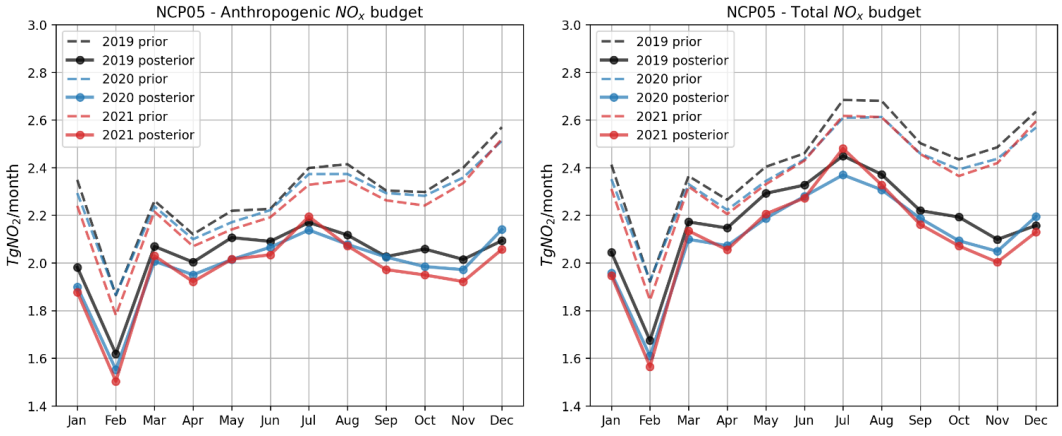


Figure 9. Times series of the monthly prior (in dashed lines) and posterior (in solid lines) for the anthropogenic (a) and total (b, anthropogenic + natural) NO_x budgets over Eastern China for the years 2019 (black), 2020 (blue) and 2021 (red), expressed in Tg equivalent NO_2 per month.

In contrast with the prior estimate of the anthropogenic emissions (Section 2.2) showing an increase of emissions throughout the year from April to December, the posterior estimates show a flatter seasonal cycle (Figure 9a). The summer peak in the prior and in DECSO can be explained by the increased electricity consumption during hot weather and the resulting power load, as (Zhang et al., 2019) shows that electricity consumption and rising temperatures are correlated. In agreement with the prior estimates, the posterior emissions show a minimum in February each year which can be linked to the LNY.

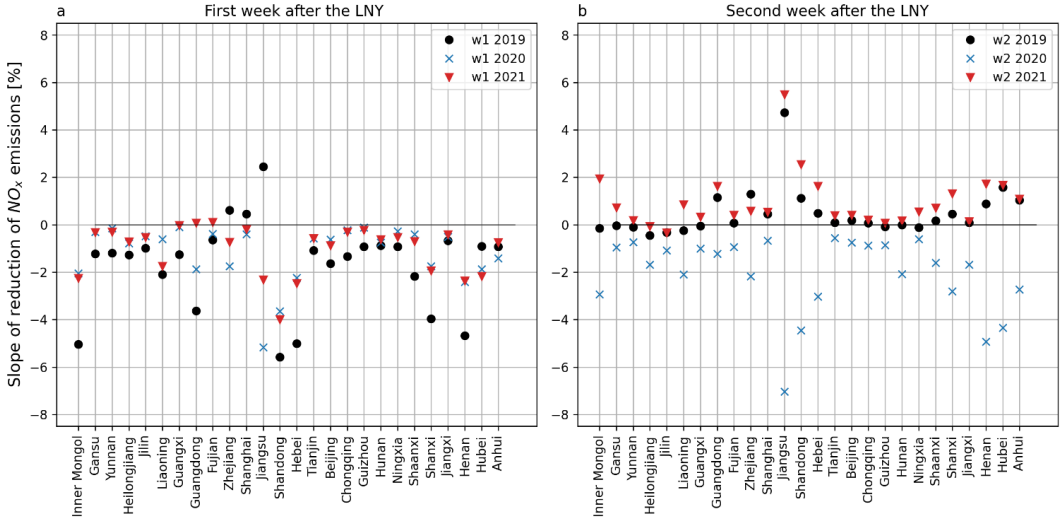
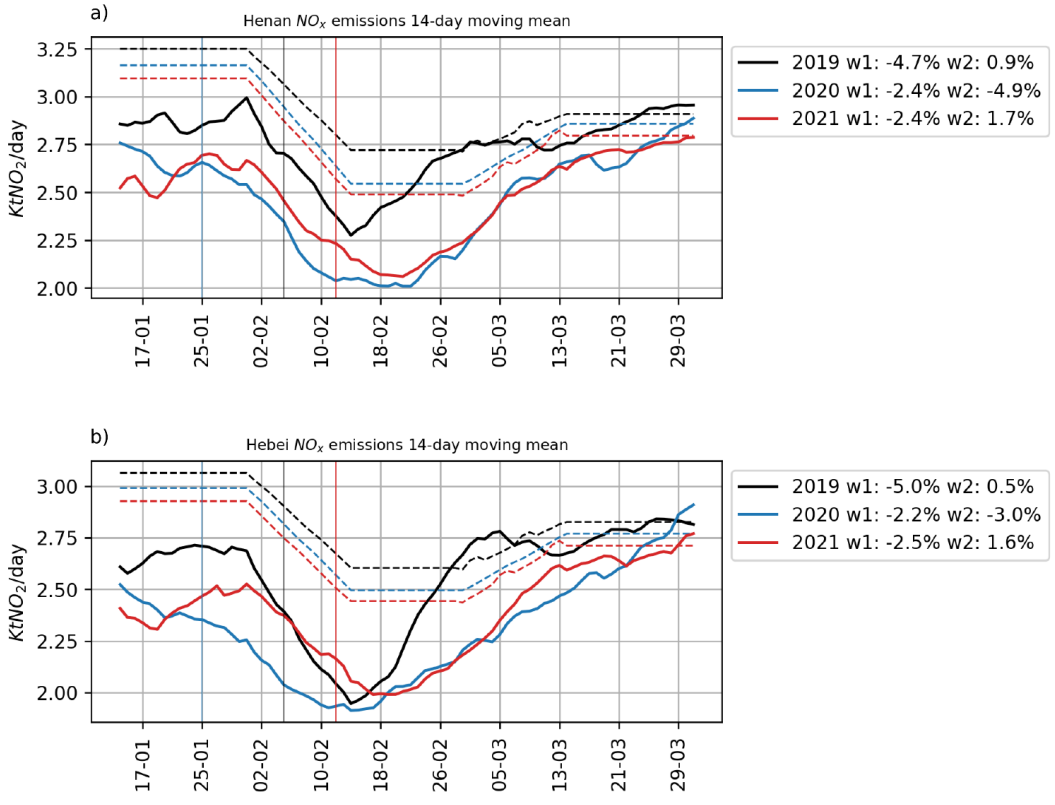


Figure 10. Slope of change in the posterior estimates of NO_x emissions during the first (a) and second (b) weeks following the LNY dates, in 2019, 2020, and 2021 in the Chinese provinces. These slopes of change are calculated for each week separately by computing the slope of a line that connects the first and the last days of the week in question. Week1 of LNY starts on the first day of the New Year for the corresponding year (assigned day1), and week2 starts on day 8. Note that the LNY dates for each year are different; and they fall on 5 February 2019, 25 January 2020, and 12 February 2021; therefore,

https://doi.org/10.5194/egusphere-2026-6638
Preprint. Discussion started: 10 November 2026
© Author(s) 2026. CC BY 4.0 License.

day 1 is assigned for each year based on the corresponding date, i.e. day1 for 2019 falls on 5 February, and for 2020 on 25 January.

Our posterior estimates show a consistent relative reduction in NO_x emissions during the first week after LNY in 2019, 2020 and 2021 for most provinces varying between -6% and -0.1% (**Figure 10**). In all provinces, the emissions rebound in the second week during 2019 and 2021, but not in 2020, with reductions between -7% and -0.1% (**Figure 10**). We also looked at the 14-day moving means of NO_x emissions in all provinces, but we show only two in **Figure 11**, Henan and Hebei, as both are some of the most densely populated provinces in China (about 99 and 75 million inhabitants, respectively, in 2020). During the first week following the LNY date in 2020, we observe reductions of NO_x emissions, that are around -5%, -2.1%, and -2.1% in Jiangsu, Hebei and Henan respectively (**Figure 11**a). These reductions are explained by the reduced industrial activities during the LNY holidays. After this decline in emissions, the activity goes back to normal, which is reflected by the rebound in NO_x emissions during the second week following the LNY date in 2019 and 2021 (**Figure 11**), but not in 2020, where we observe reductions of -7%, -3%, and -5% for all three provinces respectively, which emphasizes the influence of pandemic-related disruptions on NO_x emissions (see **Section 3.4**). Miyazaki et al. (Li et al., 2024a) showed that nearly 80% of the emission reductions, during the period 23 Jan – 29 Feb 2020, are due to the lockdown measures in each province. The outdoor restrictions took effect 9 days after the LNY in Henan, falling on 3 February 2020, and 13 days after LNY in Hebei (7 February 2020).

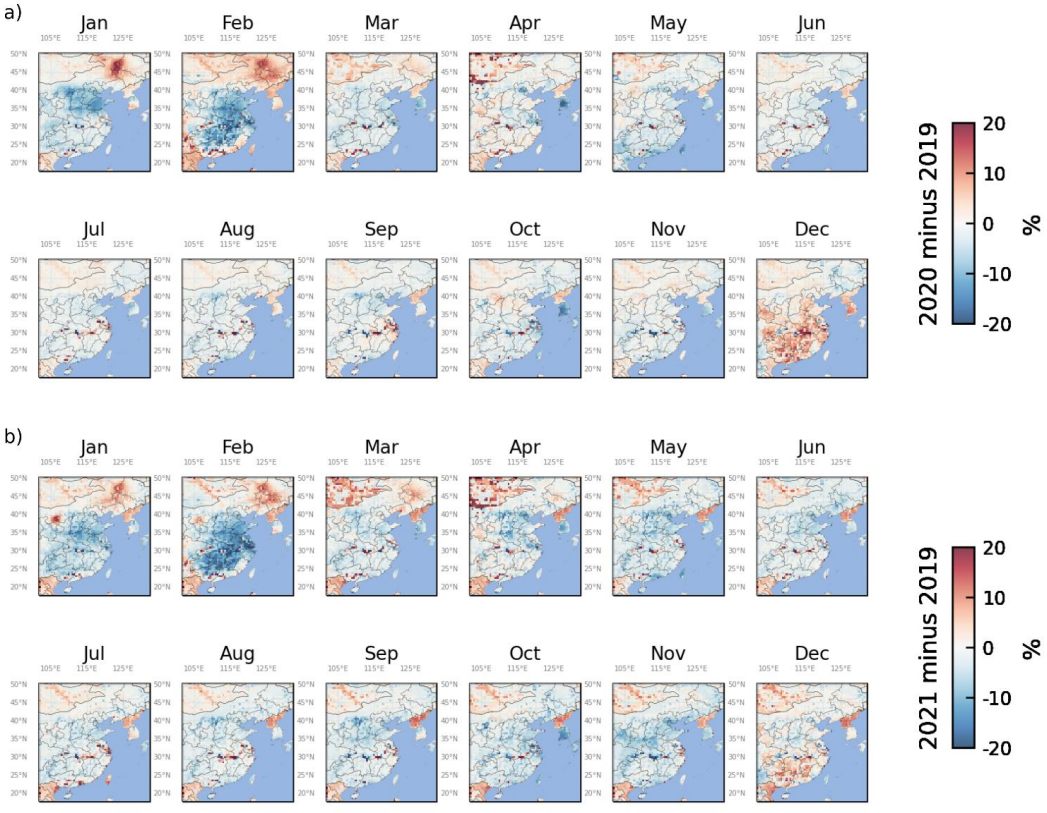


https://doi.org/10.5194/egusphere-2026-6638
Preprint. Discussion started: 10 November 2026
© Author(s) 2026. CC BY 4.0 License.

Figure 11. NO_x emissions during the early period of the year, during 2019 (black), 2020 (blue) and 2021 (red). The dotted lines are the prior estimates, and the solid lines are the posterior (corrected) estimates presented as 14-day moving means, for the province of Henan (a) and Hebei (b). In the legend, we show the slope of change during the first (w1) and the second (w2) weeks following the new year date. The Lunar New Year dates are shown as horizontal lines in black (for 2019), blue (2020) and red (2021). The slopes of change are calculated on a section of the line (for the posterior estimates). For instance, to get the slopes of week 1, we take the first and last days of the week, we then calculate the slope on a line that connects these two days; it is finally presented as a percentage of change from day 1 to day 7 during the week. The same calculation is applied for week 2, when we take the eighth day after the New Year date, and we count 7 days (day 8 to 14).

3.4. Impact of the COVID-19 lockdown and economic changes on NO_x emissions

Following a usual diagnostic in the literature to assess the change in air pollutant concentrations and emissions due to COVID-19 policies, we characterize the impact of the COVID-19 lockdown in Eastern China in terms of changes in anthropogenic emission estimates from 2019 to 2020 (Fig 12a). While Eastern China anthropogenic emissions decrease by about −1.0% in 2020 compared to 2019 in the (prior) CAMS-GLOB-ANT-v5.3 inventory, the posterior emissions show a higher decrease of about −2.3% (**Figure 7**), which is more consistent with the percentage estimated by Li et al. (Li et al., 2024b) at −2.7% in 2020 compared to 2019.



https://doi.org/10.5194/egusphere-2026-6638
Preprint. Discussion started: 10 November 2026
© Author(s) 2026. CC BY 4.0 License.

Figure 12. Relative difference (in %) in the posterior estimates of the 0.5° resolution NO_x monthly emission maps during 2020 (a) and 2021 (b) as compared to 2019, over the domain of study. Each plot is the result of the following equation: $\frac{emissions_{year} - emissions_{2019}}{emissions_{2019}} \times 100$, with $emissions_{year}$ being the posterior monthly emissions of the year in question.

February marks the month that witnessed the highest decrease in NO_x emissions: −35% in 2020 compared to 2019. This result agrees with other studies. Zheng et al. (2021) for instance found a decrease of about −36% of the NO_x emissions, leading to a good agreement between NO_2 surface observations and simulations. Miyazaki et al. (Miyazaki et al., 2020) found that Chinese NO_x emissions were reduced by −36% from early January to mid-February in 2020 compared to 2019. Finally, Kong et al. (2023) also found a decrease of about −40% of the NO_x emissions in February 2020 compared to 2019.

Our configuration allows us to access the spatial distribution of emissions variations. We observe a decrease in emissions in February (2020 and 2021) concentrated in big cities rather than rural areas, suggesting a lower mobility in big cities compared to rural regions during LNY (**Figure 12**). At the provincial resolution, the changes in emissions compared to 2019 are between -4% and +6% in 2020, and between -6% and +6% in 2021 (Figure 14). In February 2020, the reduction of emissions occurred in most of Eastern China (**Figure 12**a). The highest decrease of NOx emissions, by more than −15% (±2%), are found in the provinces of Shanghai, Hubei and Jiangsu (**Figure 13**). On the contrary, emissions increase in the three northeastern provinces of Heilongjiang, Jilin and Liaoning, and in Guangxi (southern China) (**Figure 13**). This result agrees with the study of Li et al. (2024b) also finding an increase in NO_x emissions in these three provinces, due to an increase in industrial production.

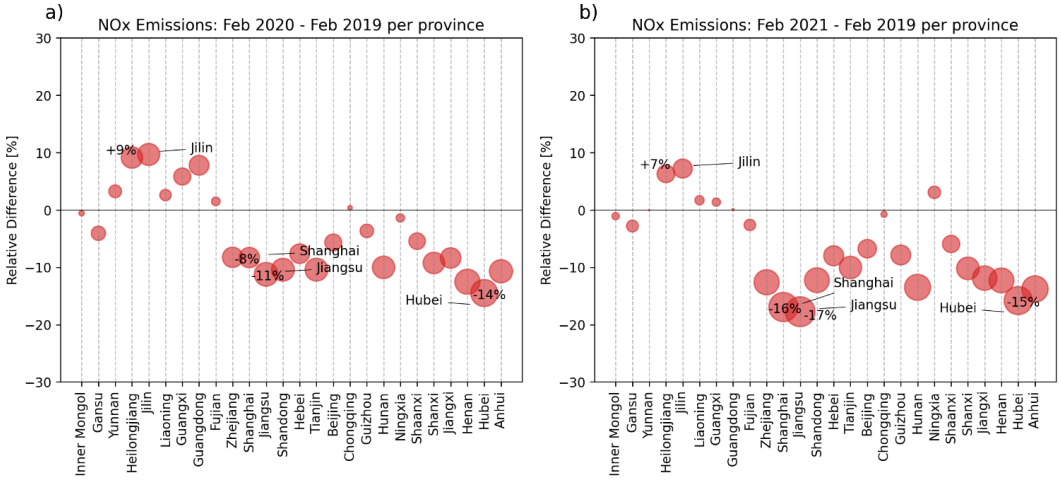


Figure 13. Relative difference in the posterior NO_x emissions during February 2020 (a) and 2021 (b) as compared to 2019, in %, for the provinces illustrated in Figure 1. Note that the scale of the y axes is not the same.

https://doi.org/10.5194/egusphere-2026-6638
Preprint. Discussion started: 10 November 2026
© Author(s) 2026. CC BY 4.0 License.

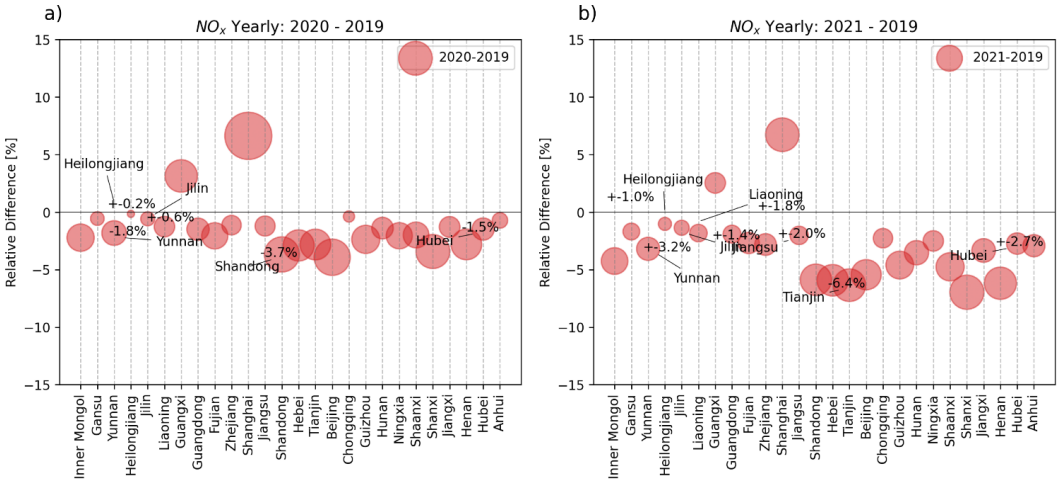


Figure 14. Same as **Figure 13**, but at the annual scale.

4. Conclusions

Monitoring past NO_x emissions allows us to assess existing air quality policies, and plan for future adaptations. In addition to BU approaches (inventories and process-based models), the assimilation of atmospheric data in inverse modeling systems can provide a means for monitoring emissions at a finer temporal resolution. This study evaluates the potential of satellite data from TROPOMI to provide estimates of NO_x emissions in Eastern China at the monthly, national and provincial scales, using regional-scale atmospheric inversions. TROPOMI NO_2 TVCDs are assimilated in the variational inversion model of the Community Inversion Framework (CIF), coupled to the CHIMERE regional CTM, and its adjoint model. We focused on the changes of NOx emissions from 2019 to 2021 in Eastern China, with an analysis of the impacts of the Chinese Lunar New Year (LNY) during the period of study, and of the COVID-19 outbreak in 2020. The LNY holidays led to a reduction of emissions during the first week following New Year Day and to an increase of emissions during the second week except in 2020. Driven by the impact of the LNY combined with the COVID-19 outbreak and the associated lockdown measures, our estimates show a reduction in NOx emissions of -35% in February 2020 relative to 2019, in Eastern China, which agrees with previous studies. NOx emissions decreased in all studied provinces, in February 2020, except industrial provinces in the Northeastern part of China. Posterior anthropogenic NOx emissions over Eastern China were about 11% lower than the prior inventory in every year from 2019 to 2021. This suggests the inventory overestimates emissions, with the largest corrections in dense urban provinces and a small further decline of about -2.2% from 2019 to 2020 that includes the COVID-19 lockdown and continues into 2021. Our estimates agree with those from DECSO (within −7.5%) and ABaCAS-EI v2.0 (within +12%), i.e. lower than DECSO and higher than ABaCAS-EI v2.0. Robust uncertainty characterization and comparison with independent datasets remain essential. By studying the changes in NOx emissions in recent past years, our dataset can help guide the design of future strategies and policies aimed at reducing NOx emissions, in China and in each province. Nevertheless, inversion-based emission estimates are governed by uncertainties linked to the data being assimilated, such as NO2 satellite observations, as well as model errors including

https://doi.org/10.5194/egusphere-2026-6638
Preprint. Discussion started: 10 November 2026
© Author(s) 2026. CC BY 4.0 License.

those from the CTM used, and the prior estimates. These uncertainties may affect the absolute magnitude of the derived emissions more than their relative temporal variability. Further testing of different modeling configurations will help us understand how methodological parameters can affect the estimation of NOx emissions, as well as comparing against estimations generated by ground-based data approaches.

Author contributions

RA, GB and AFC conceptualized the study and carried out the results analysis. RA carried out the inversions, and the output data analysis. AFC and RA carried out the input data pre-processing. RP contributed to the preprocessing for satellite observations. IP, AB, EP developed the CIF inversion system. All the co-authors read the manuscript.

Data availability

TROPOMI-RPRO-v02.04.00 data are freely available through the website https://tropomi.gesdisc.eosdis.nasa.gov/data/S5P_TROPOMI_Level2/S5P_L2__NO2____HiR.2/. The NO_x emissions of this study are available to download through the world-emission platform https://app.world-emission.com/detail/regional/nox/nox. DECSO NOx data are available here: https://www.temis.nl/emissions/region_asia/datapage.php. ABaCAS-EI v2.0 NO_x data are available here https://figshare.com/articles/dataset/Emission_trends_of_air_pollutants_and_CO2_in_China_from_2005_to_2021/21777005/1. CAMS-GLOB-ANT and CAMS-GLOB-SOIL data can be downloaded through the ECCAD plateform https://eccad.sedoo.fr/#/catalogue.

Code availability

The CHIMERE code is available here: http://www.lmd.polytechnique.fr/chimere/ (Menut et al., 2013; Mailler et al., 2017). The CIF inversion system (Berchet et al., 2021) is available at https://doi.org/10.5281/zenodo.6304912 (Berchet et al., 2022).

Financial support

A large part of the development and analysis were conducted in the frame of the World Emission project funded by the European Space Agency (ESA). This study has also received funding from the French ANR project ARGONAUT under grant agreement No ANR-19-CE01-0007, from the TOSCA ARGOS project (Centre National d'Etudes Spatiales CNES) and from the French PRIMEQUAL project LOCKAIR under grant agreement No 2162D0010.

Acknowledgements

We acknowledge the TROPOMI group for the production of the NO_2 retrievals. We wish to thank all the people involved in the preparation, coordination and management of the ESA World Emission project. Finally, we wish to thank Julien Bruna (LSCE) and his team for computer support. This work

https://doi.org/10.5194/egusphere-2026-6638
Preprint. Discussion started: 10 November 2026
© Author(s) 2026. CC BY 4.0 License.

was granted access to the HPC resources of TGCC under the allocations A0180102201 and A0190102201 made by GENCI. We acknowledge the usage of ChatGPT and Perplexity AI to generate bits of python scripts that helped with plotting some of the figures, and for rephrasing certain sentences; in both cases we reviewed and edited the outputs, and no content was used as is.

Competing Interests

The authors declare that they have no conflict of interest.

References

Abdelwahab, M. M., A. Shalaby, O., Semary, H. E., and Abonazel, M. R.: Driving Factors of NOx Emissions in China: Insights from Spatial Regression Analysis, Atmosphere 2024, Vol. 15, Page 793, 15, 793, https://doi.org/10.3390/ATMOS15070793 , 2024.

Agathokleous, E., Feng, Z., Oksanen, E., Sicard, P., Wang, Q., Saitanis, C. J., Araminiene, V., Blande, J. D., Hayes, F., Calatayud, V., Domingos, M., Veresoglou, S. D., Peñuelas, J., Wardle, D. A., de Marco, A., Li, Z., Harmens, H., Yuan, X., Vitale, M., and Paoletti, E.: Ozone affects plant, insect, and soil microbial communities: A threat to terrestrial ecosystems and biodiversity, Sci. Adv., 6, https://doi.org/10.1126/sciadv.abc1176, 2020.

Atkinson, R.: Atmospheric chemistry of VOCs and NOx, Atmos. Environ., 34, 2063–2101, https://doi.org/10.1016/S1352-2310(99)00460-4 , 2000.

Bauwens, M., Compernolle, S., Stavrakou, T., Müller, J. F., van Gent, J., Eskes, H., Levelt, P. F., van der A, R., Veefkind, J. P., Vlietinck, J., Yu, H., and Zehner, C.: Impact of Coronavirus Outbreak on NO2 Pollution Assessed Using TROPOMI and OMI Observations, Geophys. Res. Lett., 47, e2020GL087978, https://doi.org/10.1029/2020GL087978 , 2020.

Berchet, A., Sollum, E., Thompson, R. L., Pison, I., Thanwerdas, J., Broquet, G., Chevallier, F., Aalto, T., Berchet, A., Bergamaschi, P., Brunner, D., Engelen, R., Fortems-Cheiney, A., Gerbig, C., Groot Zwaaftink, C. D., Haussaire, J.-M., Henne, S., Houweling, S., Karstens, U., Kutsch, W. L., Luijkx, I. T., Monteil, G., Palmer, P. I., van Peet, J. C. A., Peters, W., Peylin, P., Potier, E., Rödenbeck, C., Saunois, M., Scholze, M., Tsuruta, A., and Zhao, Y.: The Community Inversion Framework v1.0: a unified system for atmospheric inversion studies, Geosci. Model Dev., 14, 5331–5354, https://doi.org/10.5194/gmd-14-5331-2021 , 2021.

Bo, X., Jia, M., Xue, X., Tang, L., Mi, Z., Wang, S., Cui, W., Chang, X., Ruan, J., Dong, G., Zhou, B., and Davis, S. J.: Effect of strengthened standards on Chinese ironmaking and steelmaking emissions, Nature Sustainability 2021 4:9, 4, 811–820, https://doi.org/10.1038/s41893-021-00736-0, 2021.

Bovensmann, H., Burrows, J. P., Buchwitz, M., Frerick, J., Noël, S., Rozanov, V. V., Chance, K. V., and Goede, A. P. H.: SCIAMACHY: Mission Objectives and Measurement Modes, J. Atmos. Sci., 56, 127–150, https://doi.org/10.1175/1520-0469(1999)056<0127:SMOAMM>2.0.CO;2, 1999.

Bressler, R. D.: The mortality cost of carbon, Nature Communications 2021 12:1, 12, 4467-, https://doi.org/10.1038/s41467-021-24487-w , 2021.

Burrows, J. P., Weber, M., Buchwitz, M., Rozanov, V., Ladstätter-Weißenmayer, A., Richter, A., DeBeek, R., Hoogen, R., Bramstedt, K., Eichmann, K.-U., Eisinger, M., and Perner, D.: The Global Ozone Monitoring Experiment (GOME): Mission Concept and First Scientific Results, J. Atmos. Sci., 56, 151–175, https://doi.org/10.1175/1520-0469(1999)056<0151:TGOMEG>2.0.CO;2, 1999.

Carter, W. P. L.: A detailed mechanism for the gas-phase atmospheric reactions of organic compounds, Atmospheric Environment. Part A. General Topics, 24, 481–518, https://doi.org/10.1016/0960-1686(90)90005-8, 1990.

ChinaPower. (2025). *Measuring China's Manufacturing Might | ChinaPower Project*. https://chinapower.csis.org/tracker/china-manufacturing/

Chinazzi, M., Davis, J. T., Ajelli, M., Gioannini, C., Litvinova, M., Merler, S., Pastore y Piontti, A., Mu, K., Rossi, L., Sun, K., Viboud, C., Xiong, X., Yu, H., Elizabeth Halloran, M., Longini, I. M., & Vespignani, A. (2020). The effect of travel restrictions on the spread of the 2019 novel coronavirus (COVID-19) outbreak. *Science*, *368*(6489), 395–400. https://doi.org/10.1126/science.aba9757

Chu, B., Zhang, S., Liu, J., Ma, Q., and He, H.: Significant concurrent decrease in PM2.5 and NO2 concentrations in China during COVID-19 epidemic, Journal of Environmental Sciences, 99, 346–353, https://doi.org/10.1016/J.JES.2020.06.031, 2021.

Ciarelli, G., Theobald, M. R., Vivanco, M. G., Beekmann, M., Aas, W., Andersson, C., Bergström, R., Manders-Groot, A., Couvidat, F., Mircea, M., Tsyro, S., Fagerli, H., Mar, K., Raffort, V., Roustan, Y., Pay, M. T., Schaap, M.,

https://doi.org/10.5194/egusphere-2026-6638
Preprint. Discussion started: 10 November 2026
© Author(s) 2026. CC BY 4.0 License.

Kranenburg, R., Adani, M., Briganti, G., Cappelletti, A., D'Isidoro, M., Cuvelier, C., Cholakian, A., Bessagnet, B., Wind, P., and Colette, A.: Trends of inorganic and organic aerosols and precursor gases in Europe: insights from the EURODELTA multi-model experiment over the 1990–2010 period, Geosci. Model Dev., 12, 4923–4954, https://doi.org/10.5194/GMD-12-4923-2019, 2019.

Cooper, M. J., Martin, R. V., Hammer, M. S., Levelt, P. F., Veefkind, P., Lamsal, L. N., Krotkov, N. A., Brook, J. R., and McLinden, C. A.: Global fine-scale changes in ambient NO2 during COVID-19 lockdowns, Nature 2022 601:7893, 601, 380–387, https://doi.org/10.1038/s41586-021-04229-0, 2022.

Derognat, C., Beekmann, M., Baeumle, M., Martin, D., and Schmidt, H.: Effect of natural volatile organic compound emissions on tropospheric chemistry during the Atmospheric Pollution Over the Paris Area (ESQUIF) campaign in the Ile-de-France region, Journal of Geophysical Research: Atmospheres, 108, https://doi.org/10.1029/2001JD001421, 2003.

Ding, J., Miyazaki, K., Van Der A, R. R., Mijling, B., Kurokawa, J. I., Cho, S. Y., Janssens-Maenhout, G., Zhang, Q., Liu, F., and Felicitas Levelt, P.: Intercomparison of NO_x emission inventories over East Asia, Atmos. Chem. Phys., 17, 10125–10141, https://doi.org/10.5194/ACP-17-10125-2017, 2017a.

Ding, J., van der A, R. J., Mijling, B., and Levelt, P. F.: Space-based NO $_x$ emission estimates over remote regions improved in DECSO, Atmos. Meas. Tech., 10, 925–938, https://doi.org/10.5194/amt-10-925-2017, 2017b.

Ding, J., van der A, R. J., Eskes, H. J., Mijling, B., Stavrakou, T., van Geffen, J. H. G. M., and Veefkind, J. P.: NOx Emissions Reduction and Rebound in China Due to the COVID-19 Crisis, Geophys. Res. Lett., 47, e2020GL089912, https://doi.org/10.1029/2020GL089912, 2020.

Donzelli, G. and Suarez-Varela, M. M.: Tropospheric Ozone: A Critical Review of the Literature on Emissions, Exposure, and Health Effects, Atmosphere 2024, Vol. 15, Page 779, 15, 779, https://doi.org/10.3390/ATMOS15070779 , 2024.

Eskes, H. J., Van Velthoven, P. F. J., Valks, P. J. M., and Kelder, H. M.: Assimilation of GOME total-ozone satellite observations in a three-dimensional tracer-transport model, Quarterly Journal of the Royal Meteorological Society, 129, 1663–1681, https://doi.org/10.1256/QJ.02.14, 2003.

Fengxia, G., Min, B., Yijun, M., Zupei, L., Yawen, L., and Haifeng, S.: Temporal and spatial characteristics of lightning-produced nitrogen oxides in China, J. Atmos. Sol. Terr. Phys., 149, 100–107, https://doi.org/10.1016/J.JASTP.2016.10.007, 2016.

Fortems-Cheiney, A., Pison, I., Broquet, G., Dufour, G., Berchet, A., Potier, E., Coman, A., Siour, G., and Costantino, L.: Variational regional inverse modeling of reactive species emissions with PYVAR-CHIMERE-v2019, Geosci. Model Dev., 14, 2939–2957, https://doi.org/10.5194/GMD-14-2939-2021, 2021.

Fortems-Cheiney, A., Broquet, G., Potier, E., Plauchu, R., Berchet, A., Pison, I., Denier van der Gon, H., and Dellaert, S.: CO anthropogenic emissions in Europe from 2011 to 2021: insights from Measurement of Pollution in the Troposphere (MOPITT) satellite data, Atmos. Chem. Phys., 24, 4635–4649, https://doi.org/10.5194/acp-24-4635-2024, 2024.

Fortems-Cheiney, A., Broquet, G., Potier, E., Berchet, A., Pison, I., Martinez, A., Plauchu, R., Abeed, R., Sicsik-Paré, A., Dufour, G., Coman, A., Savas, D., Siour, G., Eskes, H., Denier van der Gon, H. A. C., and Dellaert, S. N. C.: Assessing the ability to quantify the decrease in NOx anthropogenic emissions in 2019 compared to 2005 using OMI and TROPOMI satellite observations, Atmos. Chem. Phys., 25, 6047–6068, https://doi.org/10.5194/ACP-25-6047-2025, 2025.

Gao, C., Zhang, X., Xiu, A., Tong, Q., Zhao, H., Zhang, S., Yang, G., Zhang, M., and Xie, S.: Intercomparison of multiple two-way coupled meteorology and air quality models (WRF v4.1.1-CMAQ v5.3.1, WRF-Chem v4.1.1, and WRF v3.7.1-CHIMERE v2020r1) in eastern China, Geosci. Model Dev., 17, 2471–2492, https://doi.org/10.5194/GMD-17-2471-2024, 2024.

Gao, M., Xing, Z., Vollrath, C., Hugenholtz, C. H., and Barchyn, T. E.: Global observational coverage of onshore oil and gas methane sources with TROPOMI, Scientific Reports 2023 13:1, 13, 16759-, https://doi.org/10.1038/s41598-023-41914-8, 2023.

Van Geffen, J., Eskes, H., Compernolle, S., Pinardi, G., Verhoelst, T., Lambert, J. C., Sneep, M., Linden, M. Ter, Ludewig, A., Folkert Boersma, K., and Pepijn Veefkind, J.: Sentinel-5P TROPOMI NO_2 retrieval: impact of version v2.2 improvements and comparisons with OMI and ground-based data, Atmos. Meas. Tech., 15, 2037–2060, https://doi.org/10.5194/AMT-15-2037-2022, 2022.

Gu, D., Wang, Y., Smeltzer, C., and Boersma, K. F.: Anthropogenic emissions of NOx over China: Reconciling the difference of inverse modeling results using GOME-2 and OMI measurements, Journal of Geophysical Research: Atmospheres, 119, 7732–7740, https://doi.org/10.1002/2014JD021644, 2014.

Guenther, A., Karl, T., Harley, P., Wiedinmyer, C., Palmer, P. I., and Geron, C.: Estimates of global terrestrial isoprene emissions using MEGAN (Model of Emissions of Gases and Aerosols from Nature), Atmos. Chem. Phys., 6, 3181–3210, https://doi.org/10.5194/ACP-6-3181-2006, 2006.

He, H., Wang, Y., Ma, Q., Ma, J., Chu, B., Ji, D., Tang, G., Liu, C., Zhang, H., and Hao, J.: Mineral dust and NOx promote the conversion of SO2 to sulfate in heavy pollution days, Scientific Reports 2014 4:1, 4, 4172-, https://doi.org/10.1038/srep04172, 2014.

https://doi.org/10.5194/egusphere-2026-6638
Preprint. Discussion started: 10 November 2026
© Author(s) 2026. CC BY 4.0 License.

He, T. L., Jones, D. B. A., Miyazaki, K., Bowman, K. W., Jiang, Z., Chen, X., Li, R., Zhang, Y., and Li, K.: Inverse modelling of Chinese NOxemissions using deep learning: integrating in situ observations with a satellite-based chemical reanalysis, Atmos. Chem. Phys., 22, 14059–14074, https://doi.org/10.5194/ACP-22-14059-2022, 2022.

Herman, J., Cede, A., Spinei, E., Mount, G., Tzortziou, M., and Abuhassan, N.: NO2 column amounts from ground-based Pandora and MFDOAS spectrometers using the direct-sun DOAS technique: Intercomparisons and application to OMI validation, Journal of Geophysical Research: Atmospheres, 114, 13307, https://doi.org/10.1029/2009JD011848, 2009.

HKTDC. (2026). HKTDC Research - Data and Profiles - Chinese Mainland Provinces and Cities - Provinces - Wuhan City Information. https://research.hktdc.com/en/data-and-profiles/mcpc/provinces/hubei/wuhan, last access: 10 November 2026.

Jena, C., Ghude, S. D., Beig, G., Chate, D. M., Kumar, R., Pfister, G. G., Lal, D. M., Surendran, D. E., Fadnavis, S., and van der A, R. J.: Inter-comparison of different NOX emission inventories and associated variation in simulated surface ozone in Indian region, Atmos. Environ., 117, 61–73, https://doi.org/10.1016/J.ATMOSENV.2015.06.057 , 2015.

Ju, K., Lu, L., Wang, W., Chen, T., Yang, C., Zhang, E., Xu, Z., Li, S., Song, J., Pan, J., and Guo, Y.: Causal effects of air pollution on mental health among Adults——An exploration of susceptible populations and the role of physical activity based on a longitudinal nationwide cohort in China, Environ. Res., 217, 114761, https://doi.org/10.1016/J.ENVRES.2022.114761, 2023.

Kong, L., Tang, X., Zhu, J., Wang, Z., Sun, Y., Fu, P., Gao, M., Wu, H., Lu, M., Wu, Q., Huang, S., Sui, W., Li, J., Pan, X., Wu, L., Akimoto, H., and Carmichael, G. R.: Unbalanced emission reductions of different species and sectors in China during COVID-19 lockdown derived by multi-species surface observation assimilation, Atmos. Chem. Phys., 23, 6217–6240, https://doi.org/10.5194/ACP-23-6217-2023, 2023.

Lambert, J.-C., Keppens, A., Compernolle, S., Eichmann, K.-U., de Graaf, M., Hubert, D., Langerock, B., Sha, M. K., van der Plas, E., Verhoelst, T., Wagner, T., Ahn, C., Argyrouli, A., Balis, D., Chan, K. L., Coldewey-Egbers, M., de Smedt, I., Eskes, H., Fjæraa, A. M., … Weber, M. (2025). Copernicus Atmospheric Mission Performance Cluster Service Quarterly Validation Report of the Copernicus Sentinel-5 Precursor Operational Data Products #26: April 2018-February 2025 (Issue 26). https://s5p-mpc-vdaf.aeronomie.be/ProjectDir/reports//pdf/S5P-MPC-IASB-ROCVR-26.01.00_FINAL.pdf

Levelt, P. F., Joiner, J., Tamminen, J., Veefkind, J. P., Bhartia, P. K., Stein Zweers, D. C., Duncan, B. N., Streets, D. G., Eskes, H., van der A, R., McLinden, C., Fioletov, V., Carn, S., de Laat, J., DeLand, M., Marchenko, S., McPeters, R., Ziemke, J., Fu, D., Liu, X., Pickering, K., Apituley, A., González Abad, G., Arola, A., Boersma, F., Chan Miller, C., Chance, K., de Graaf, M., Hakkarainen, J., Hassinen, S., Ialongo, I., Kleipool, Q., Krotkov, N., Li, C., Lamsal, L., Newman, P., Nowlan, C., Suleiman, R., Tilstra, L. G., Torres, O., Wang, H., and Wargan, K.: The Ozone Monitoring Instrument: overview of 14 years in space, Atmos. Chem. Phys., 18, 5699–5745, https://doi.org/10.5194/acp-18-5699-2018, 2018.

Levelt, P. F., Stein Zweers, D. C., Aben, I., Bauwens, M., Borsdorff, T., De Smedt, I., Eskes, H. J., Lerot, C., Loyola, D. G., Romahn, F., Stavrakou, T., Theys, N., Van Roozendael, M., Veefkind, J. P., and Verhoelst, T.: Air quality impacts of COVID-19 lockdown measures detected from space using high spatial resolution observations of multiple trace gases from Sentinel-5P/TROPOMI, Atmos. Chem. Phys., 22, 10319–10351, https://doi.org/10.5194/ACP-22-10319-2022, 2022.

Li, H., Zheng, B., Lei, Y., Hauglustaine, D., Chen, C., Lin, X., Zhang, Y., Zhang, Q., and He, K.: Trends and drivers of anthropogenic NOx emissions in China since 2020, Environmental Science and Ecotechnology, 21, 100425, https://doi.org/10.1016/J.ESE.2024.100425, 2024a.

Li, H., Qiu, J., and Zheng, B.: Air-pollution-satellite-based CO_2 emission inversion: system evaluation, sensitivity analysis, and future research direction, Atmos. Chem. Phys., 25, 1949–1963, https://doi.org/10.5194/ACP-25-1949-2025, 2025.

Li, Q., Guo, F., Ju, X., Liu, Z., Gan, M., Zhang, K., and Cai, B.: Estimation of Lightning-Generated NOx in the Mainland of China Based on Cloud-to-Ground Lightning Location Data, Adv. Atmos. Sci., 40, 129–143, https://doi.org/10.1007/s00376-022-1329-6, 2023a.

Li, R., Pei, S., Chen, B., Song, Y., Zhang, T., Yang, W., and Shaman, J.: Substantial undocumented infection facilitates the rapid dissemination of novel coronavirus (SARS-CoV-2), Science (1979)., 368, 489–493, DOI:10.1126/science.abb3221, 2020.

Li, R., Gao, Y., Han, Y., Zhang, Y., Zhang, B., Fu, H., and Wang, G.: RETRACTED: Elucidating the mechanisms of rapid O3 increase in North China Plain during COVID-19 lockdown period, Science of The Total Environment, 906, 167622, https://doi.org/10.1016/J.SCITOTENV.2023.167622, 2024b.

Li, S., Wang, S., Wu, Q., Zhang, Y., Ouyang, D., Zheng, H., Han, L., Qiu, X., Wen, Y., Liu, M., Jiang, Y., Yin, D., Liu, K., Zhao, B., Zhang, S., Wu, Y., and Hao, J.: Emission trends of air pollutants and CO2 in China from 2005 to 2021, Earth Syst. Sci. Data, 15, 2279–2294, https://doi.org/10.5194/ESSD-15-2279-2023, 2023b.

Li, S., Wang, S., Wu, Q., Zhang, Y., Ouyang, D., Zheng, H., Han, L., Qiu, X., Wen, Y., Liu, M., Jiang, Y., Yin, D., Liu, K., Zhao, B., Zhang, S., Wu, Y., and Hao, J.: Emission trends of air pollutants and CO2 in China from 2005 to 2021, Earth Syst. Sci. Data, 15, 2279–2294, https://doi.org/10.5194/ESSD-15-2279-2023, 2023c.

https://doi.org/10.5194/egusphere-2026-6638
Preprint. Discussion started: 10 November 2026
© Author(s) 2026. CC BY 4.0 License.

Liu, F., Beirle, S., Joiner, J., Choi, S., Tao, Z., Knowland, K. E., Smith, S. J., Tong, D. Q., Ma, S., Fasnacht, Z. T., and Wagner, T.: High-resolution mapping of nitrogen oxide emissions in large US cities from TROPOMI retrievals of tropospheric nitrogen dioxide columns, Atmos. Chem. Phys., 24, 3717–3728, https://doi.org/10.5194/ACP-24-3717-2024, 2024.

Liu, J., Tong, D., Zheng, Y., Cheng, J., Qin, X., Shi, Q., Yan, L., Lei, Y., and Zhang, Q.: Carbon and air pollutant emissions from China's cement industry 1990-2015: Trends, evolution of technologies, and drivers, Atmos. Chem. Phys., 21, 1627–1647, https://doi.org/10.5194/ACP-21-1627-2021, 2021.

Lu, B., Zhang, Z., Jiang, J., Meng, X., Liu, C., Herrmann, H., Chen, J., Xue, L., and Li, X.: Unraveling the O3-NOX-VOCs relationships induced by anomalous ozone in industrial regions during COVID-19 in Shanghai, Atmos. Environ., 308, 119864, https://doi.org/10.1016/J.ATMOSENV.2023.119864, 2023.

Menut, L., Bessagnet, B., Siour, G., Mailler, S., Pennel, R., and Cholakian, A.: Impact of lockdown measures to combat Covid-19 on air quality over western Europe, Science of The Total Environment, 741, 140426, https://doi.org/10.1016/J.SCITOTENV.2020.140426, 2020.

Menut, L., Cholakian, A., Pennel, R., Siour, G., Mailler, S., Valari, M., Lugon, L., and Meurdesoif, Y.: The CHIMERE chemistry-transport model v2023r1, Geosci. Model Dev., 17, 5431–5457, https://doi.org/10.5194/gmd-17-5431-2024, 2024.

Mijling, B., Van Der A, R. J., and Zhang, Q.: Regional nitrogen oxides emission trends in East Asia observed from space, Atmos. Chem. Phys., 13, 12003–12012, https://doi.org/10.5194/ACP-13-12003-2013, 2013.

Miyazaki, K., Eskes, H. J., and Sudo, K.: Global NO x emission estimates derived from an assimilation of OMI tropospheric NO 2 columns, Atmos. Chem. Phys., 12, 2263–2288, https://doi.org/10.5194/ACP-12-2263-2012, 2012.

Miyazaki, K., Bowman, K., Sekiya, T., Eskes, H., Boersma, F., Worden, H., Livesey, N., H. Payne, V., Sudo, K., Kanaya, Y., Takigawa, M., and Ogochi, K.: Updated tropospheric chemistry reanalysis and emission estimates, TCR-2, for 2005–2018, Earth Syst. Sci. Data, 12, 2223–2259, https://doi.org/10.5194/ESSD-12-2223-2020, 2020.

Munro, R., Lang, R., Klaes, D., Poli, G., Retscher, C., Lindstrot, R., Huckle, R., Lacan, A., Grzegorski, M., Holdak, A., Kokhanovsky, A., Livschitz, J., and Eisinger, M.: The GOME-2 instrument on the Metop series of satellites: instrument design, calibration, and level 1 data processing – an overview, Atmos. Meas. Tech., 9, 1279–1301, https://doi.org/10.5194/amt-9-1279-2016, 2016.

NPC: 11th Five-Year Plan (2006-2010) for National Economic and Social Development | ESCAP Policy Documents Managment, 2006. https://policy.asiapacificenergy.org/node/115

Owens, R. and Hewson, T.: ECMWF Forecast User Guide | ECMWF, https://www.ecmwf.int/en/elibrary/81307-ecmwf-forecast-user-guide, last access: 16 September 2026, 2018., 2018.

Pei, Z., Han, G., Ma, X., Su, H., and Gong, W.: Response of major air pollutants to COVID-19 lockdowns in China, Science of The Total Environment, 743, 140879, https://doi.org/10.1016/J.SCITOTENV.2020.140879, 2020.

Plauchu, R., Fortems-Cheiney, A., Broquet, G., Pison, I., Berchet, A., Potier, E., Dufour, G., Coman, A., Savas, D., Siour, G., and Eskes, H.: NO $_x$ emissions in France in 2019–2021 as estimated by the high spatial resolution assimilation of TROPOMI NO $_2$ observations, https://doi.org/10.5194/egusphere-2024-103, 19 February 2024., 2024.

Qin, K., Lu, L., Liu, J., He, Q., Shi, J., Deng, W., Wang, S., and Cohen, J. B.: Model-free daily inversion of NOx emissions using TROPOMI (MCMFE-NOx) and its uncertainty: Declining regulated emissions and growth of new sources, Remote Sens. Environ., 295, 113720, https://doi.org/10.1016/J.RSE.2023.113720, 2023.

Rijsdijk, P., Eskes, H., Dingemans, A., Boersma, K. F., Sekiya, T., Miyazaki, K., and Houweling, S.: Quantifying uncertainties in satellite NO_2 superobservations for data assimilation and model evaluation, Geosci. Model Dev., 18, 483–509, https://doi.org/10.5194/GMD-18-483-2025, 2025.

Saikawa, E., Kim, H., Zhong, M., Avramov, A., Zhao, Y., Janssens-Maenhout, G., Kurokawa, J.-I., Klimont, Z., Wagner, F., Naik, V., Horowitz, L. W., and Zhang, Q.: Comparison of emissions inventories of anthropogenic air pollutants and greenhouse gases in China, Atmos. Chem. Phys, 17, 6393–6421, https://doi.org/10.5194/acp-17-6393-2017, 2017.

Savas, D., Dufour, G., Coman, A., Siour, G., Fortems-Cheiney, A., Broquet, G., Pison, I., Berchet, A., and Bessagnet, B.: Anthropogenic NOx Emission Estimations over East China for 2015 and 2019 Using OMI Satellite Observations and the New Inverse Modeling System CIF-CHIMERE, Atmosphere (Basel)., 14, 154, https://doi.org/10.3390/atmos14010154, 2023.

Shaw, S. and Van Heyst, B.: An Evaluation of Risk Ratios on Physical and Mental Health Correlations due to Increases in Ambient Nitrogen Oxide (NOx) Concentrations, Atmosphere 2022, Vol. 13, Page 967, 13, 967, https://doi.org/10.3390/ATMOS13060967, 2022.

Simpson, D., Darras, S., and Simpson, D.: Global soil NO emissions for Atmospheric Chemical Transport Modelling: CAMS-GLOB-SOIL v2.2, Earth System Science Data Discussions, 1–35, https://doi.org/10.5194/ESSD-2021-221, 2021.

Song, M., Zhao, X., Liu, P., Mu, J., He, G., Zhang, C., Tong, S., Xue, C., Zhao, X., Ge, M., and Mu, Y.: Atmospheric NOx oxidation as major sources for nitrous acid (HONO), npj Climate and Atmospheric Science 2023 6:1, 6, 30-, https://doi.org/10.1038/s41612-023-00357-8, 2023.

Soni, V., Singh, P., Shree, V., and Goel, V.: Effects of VOCs on Human Health, Energy, Environment, and Sustainability, 119–142, https://doi.org/10.1007/978-981-10-7185-0_8, 2018.

https://doi.org/10.5194/egusphere-2026-6638
Preprint. Discussion started: 10 November 2026
© Author(s) 2026. CC BY 4.0 License.

Soulie, A., Granier, C., Darras, S., Zilbermann, N., Doumbia, T., Guevara, M., Jalkanen, J.-P., Keita, S., Liousse, C., Crippa, M., Guizzardi, D., Hoesly, R., and Smith, S. J.: Global anthropogenic emissions (CAMS-GLOB-ANT) for the Copernicus Atmosphere Monitoring Service simulations of air quality forecasts and reanalyses, Earth Syst. Sci. Data, 16, 2261–2279, https://doi.org/10.5194/essd-16-2261-2024, 2024.

Szopa, S., Foret, G., Menut, L., and Cozic, A.: Impact of large scale circulation on European summer surface ozone and consequences for modelling forecast, Atmos. Environ., 43, 1189–1195, https://doi.org/10.1016/j.atmosenv.2008.10.039, 2009.

Tan, P. H., Chou, C., Liang, J. Y., Chou, C. C. K., and Shiu, C. J.: Air pollution "holiday effect" resulting from the Chinese New Year, Atmos. Environ., 43, 2114–2124, https://doi.org/10.1016/J.ATMOSENV.2009.01.037, 2009.

Tang, L., Xue, X., Qu, J., Mi, Z., Bo, X., Chang, X., Wang, S., Li, S., Cui, W., and Dong, G.: Air pollution emissions from Chinese power plants based on the continuous emission monitoring systems network, Scientific Data 2020 7:1, 7, 325-, https://doi.org/10.1038/s41597-020-00665-1, 2020.

Tilstra, L. G., De Graaf, M., Trees, V. J. H., Litvinov, P., Dubovik, O., and Stammes, P.: A directional surface reflectance climatology determined from TROPOMI observations, Atmos. Meas. Tech., 17, 2235–2256, https://doi.org/10.5194/AMT-17-2235-2024, 2024.

Veefkind, J. P., Aben, I., McMullan, K., Förster, H., de Vries, J., Otter, G., Claas, J., Eskes, H. J., de Haan, J. F., Kleipool, Q., van Weele, M., Hasekamp, O., Hoogeveen, R., Landgraf, J., Snel, R., Tol, P., Ingmann, P., Voors, R., Kruizinga, B., Vink, R., Visser, H., and Levelt, P. F.: TROPOMI on the ESA Sentinel-5 Precursor: A GMES mission for global observations of the atmospheric composition for climate, air quality and ozone layer applications, Remote Sens. Environ., 120, 70–83, https://doi.org/10.1016/J.RSE.2011.09.027, 2012.

Visser, A. J., Boersma, K. F., Ganzeveld, L. N., and Krol, M. C.: European NO $_x$ emissions in WRF-Chem derived from OMI: impacts on summertime surface ozone, Atmos. Chem. Phys., 19, 11821–11841, https://doi.org/10.5194/acp-19-11821-2019, 2019.

Wang, T., Xue, L., Feng, Z., Dai, J., Zhang, Y., and Tan, Y.: Ground-level ozone pollution in China: a synthesis of recent findings on influencing factors and impacts, Environmental Research Letters, 17, 063003, https://doi.org/10.1088/1748-9326/AC69FE, 2022.

Wei, J., Li, Z., Wang, J., Li, C., Gupta, P., and Cribb, M.: Ground-level gaseous pollutants (NO2, SO2, and CO) in China: Daily seamless mapping and spatiotemporal variations, Atmos. Chem. Phys., 23, 1511–1532, https://doi.org/10.5194/ACP-23-1511-2023, 2023.

Yin, L., Du, P., Zhang, M., Liu, M., Xu, T., and Song, Y.: Estimation of emissions from biomass burning in China (2003-2017) based on MODIS fire radiative energy data, Biogeosciences, 16, 1629–1640, https://doi.org/10.5194/BG-16-1629-2019, 2019.

Zhang, Q., Song, Y., Li, M., and Zheng, B.: Anthropogenic emissions of SO2, NOx, and NH3 in China, Atmospheric Reactive Nitrogen in China: Emission, Deposition and Environmental Impacts, 13–40, https://doi.org/10.1007/978-981-13-8514-8_2, 2019.

Zhang, R., Zhang, Y., Lin, H., Feng, X., Fu, T. M., and Wang, Y.: NOx Emission Reduction and Recovery during COVID-19 in East China, Atmosphere 2020, Vol. 11, Page 433, 11, 433, https://doi.org/10.3390/ATMOS11040433, 2020.

Zheng, B., Tong, D., Li, M., Liu, F., Hong, C., Geng, G., Li, H., Li, X., Peng, L., Qi, J., Yan, L., Zhang, Y., Zhao, H., Zheng, Y., He, K., and Zhang, Q.: Trends in China's anthropogenic emissions since 2010 as the consequence of clean air actions, Atmos. Chem. Phys., 18, 14095–14111, https://doi.org/10.5194/ACP-18-14095-2018, 2018.

Zheng, B., Zhang, Q., Geng, G., Chen, C., Shi, Q., Cui, M., Lei, Y., and He, K.: Changes in China's anthropogenic emissions and air quality during the COVID-19 pandemic in 2020, Earth Syst. Sci. Data, 13, 2895–2907, https://doi.org/10.5194/ESSD-13-2895-2021, 2021.

Zock, J. P., Verheij, R., Helbich, M., Volker, B., Spreeuwenberg, P., Strak, M., Janssen, N. A. H., Dijst, M., and Groenewegen, P.: The impact of social capital, land use, air pollution and noise on individual morbidity in Dutch neighbourhoods, Environ. Int., 121, 453–460, https://doi.org/10.1016/J.ENVINT.2018.09.008, 2018.